

# Hořava-Lifshitz Bouncing Bianchi IX Universes: A Dynamical System Analysis

Rodrigo Maier<sup>1</sup> and Ivano Damião Soares<sup>2</sup>

<sup>1</sup> *Departamento de Física Teórica, Instituto de Física, Universidade do Estado do Rio de Janeiro, Rua São Francisco Xavier 524, Maracanã, CEP 20550-900, Rio de Janeiro, Brasil, and*

<sup>2</sup> *Centro Brasileiro de Pesquisas Físicas – CBPF,*

*Rua Dr. Xavier Sigaud, 150, Urca, CEP 22290-180, Rio de Janeiro, Brazil*

(Dated: April 27, 2022)

We examine the Hamiltonian dynamics of bouncing Bianchi IX cosmologies with three scale factors in Hořava-Lifshitz (HL) gravity. We assume a positive cosmological constant plus noninteracting dust and radiation as the matter content of the models. In this framework the modified field equations contain additional terms which turn the dynamics nonsingular. The 6-dim phase space presents (i) two critical points in a finite region of the phase space, (ii) one asymptotic de Sitter attractor at infinity and (iii) a 2-dim invariant plane containing the critical points; together they organize the dynamics of the phase space. We identified four distinct parameter domains  $A$ ,  $B$ ,  $C$  and  $D$  for which the pair of critical points engenders distinct features in the dynamics, connected to the presence of centers of multiplicity two and saddles of multiplicity two. In the domain  $A$  the dynamics consists basically of periodic bouncing orbits, or oscillatory orbits with a finite number of bounces before escaping to the de Sitter attractor. The center with multiplicity two engenders in its neighborhood the topology of stable and unstable cylinders  $R \times S^3$  of orbits, where  $R$  is a saddle direction and  $S^3$  is the center manifold of unstable periodic orbits. We show that the stable and unstable cylinders coalesce realizing a smooth homoclinic connection to the center manifold, a rare event of regular/non-chaotic dynamics in bouncing Bianchi IX cosmologies. The presence of a saddle of multiplicity two in the domain  $B$  engenders a high instability in the dynamics so that the cylinders emerging from the center manifold about  $P_2$  towards the bounce have four distinct attractors: the center manifold itself, the de Sitter attractor at infinity and two further momentum-dominated attractors with infinite anisotropy. In the domain  $C$  we examine the features of invariant manifolds of orbits about a saddle of multiplicity two  $P_2$ . The presence of the saddle of multiplicity two engenders bifurcations of the invariant manifold as the energy  $E_0$  of the system increases relative to the energy  $E_{cr_2}$  of  $P_2$ : (i) for  $E_0 < E_{cr_2}$  the invariant manifold has the topology  $S^3$ ; (ii) for  $E_0 = E_{cr_2}$  two points of  $S^3$  pinch into the point  $P_2$ , so that the invariant manifold contains infinitely many orbits homoclinic to  $P_2$ ; (iii) for  $E_0 > E_{cr_2}$  the center manifold bifurcates into a 3-torus; (iv) for  $E_0$  sufficiently large the 3-torus bifurcates into three  $S^3$ , an invariant manifold multiply connected. Such structures were not yet observed in the literature. The domain  $D$  is not examined as most of its features are present already in the previous domains.

PACS numbers: 98.80.Cq, 04.60.Ds

## I. INTRODUCTION

Although General Relativity is the most successful theory that currently describes gravitation, it presents some intrinsic crucial pathologies when one tries to construct a cosmological model of a proper theory of gravitation. In cosmology, the  $\Lambda$ CDM model gives us important predictions concerning the evolution of the Universe and about its current state [1–4]. However, let us assume that the initial conditions of our Universe were fixed when the early Universe emerged from the semi-Planckian regime and started its classical expansion. Evolving back such initial conditions using the Einstein field equations, we see that our Universe is driven towards an initial singularity where the classical regime is no longer valid [5].

Notwithstanding the cosmic censorship conjecture [6], there is no doubt that General Relativity must be properly corrected or even replaced by a completely new theory, let us say a quantum theory of gravity. This demand is in order to solve the issue of the presence of the initial singularity predicted by classical General Relativity in the beginning of the Universe.

One of the most important characteristics of our Universe supported by observational data is its homogeneity and isotropy at large scales. However, when we consider a homogeneous and isotropic model filled with baryonic matter, we find several difficulties by taking into account the primordial state of our Universe. Among such difficulties, we can mention the horizon and flatness problems [1–4]. Although the Inflationary Paradigm[7] allows one to solve problems like these, inflationary cosmology does not solve the problem of the initial singularity.

On the other hand, since 1998 [8] observational data have been giving support to the highly unexpected assumption that our Universe is currently in a state of accelerated expansion. In order to explain this state of late-time acceleration, cosmologists have been considering the existence of some field – known as dark energy – that violates the strong energy condition. Although it poses a problem to quantum field theory on how to accommodate its observed value with vacuum energy calculations[9], the cosmological constant seems to be the simplest and most appealing candidate for dark energy. Therefore, nonsingular models which provide late-time acceleration should be strongly considered.

During the last decades, bouncing models [10–13] have been considered in order to solve the problem of initial singularity predicted by General Relativity. Such models (as in [14–16]) might provide attractive alternatives to the inflationary paradigm once they can solve the horizon and flatness problems, and justify the power spectrum of primordial cosmological perturbations inferred by observations.

In 2009, P. Hořava proposed a modified gravity theory by considering a Lifshitz-type anisotropic scaling between space and time at high energies [17]. In this context, it has been shown [18, 19] that higher spatial curvature terms can lead to regular bounce solutions in the early Universe. Since its proposal, several versions of Hořava-Lifshitz gravity have emerged.

In the case of a 4-dimensional (1 + 3) spacetime, the basic assumption which is required by all the versions of Hořava-Lifshitz theories is that a preferred foliation of spacetime is *a priori* imposed. Therefore it is natural to work with the Arnowitt-Deser-Misner (ADM) decomposition of spacetime

$$ds^2 = N^2 dt^2 - {}^{(3)}g_{ij}(N^i dt + dx^i)(N^j dt + dx^j), \quad (1)$$

where  $N = N(t, x^i)$  is the lapse function,  $N^i = N^i(t, x^i)$  is the shift and  ${}^{(3)}g_{ij} = {}^{(3)}g_{ij}(t, x^i)$  is the spatial geometry. In this case the final action of the theory will not be invariant under diffeomorphisms as in General Relativity. Nevertheless, an invariant foliation preserving diffeomorphisms can be assumed. This is achieved if the action is invariant under the symmetry of time reparametrization together with time-dependent spatial diffeomorphisms. That is:

$$t \rightarrow \bar{t}(t), \quad x^i \rightarrow \bar{x}^i(t, x^i). \quad (2)$$

It turns out that the only covariant object under spatial diffeomorphisms that contains one time derivative of the spatial metric is the extrinsic curvature  $K_{ij}$

$$K_{ij} = \frac{1}{2N} \left[ \frac{\partial {}^{(3)}g_{ij}}{\partial t} - \nabla_i N_j - \nabla_j N_i \right] \quad (3)$$

where  $\nabla_i$  is the covariant derivative built with the spatial metric  ${}^{(3)}g_{ij}$ . Thus, to construct the general theory which is of second order in time derivatives, one needs to consider the quadratic terms  $K_{ij}K^{ij}$  and  $K^2$  – where  $K$  is the trace of  $K_{ij}$  – in the extrinsic curvature. By taking these terms into account we obtain the following general action

$$S_{\text{HL}} \propto \int N \sqrt{{}^{(3)}g} \left[ (K_{ij}K^{ij} - \lambda K^2 - {}^{(3)}R) - U_{\text{HL}}({}^{(3)}g_{ij}, N) \right] d^3 x dt \quad (4)$$

where  ${}^{(3)}g$  is the determinant of the spatial metric and  $\lambda$  is a constant which corresponds to a dimensionless running coupling. As in General Relativity the term  $K_{ij}K^{ij} - K^2$  is invariant under four-dimensional diffeomorphisms, we expect to recover the classical regime for

$\lambda \rightarrow 1$ . That is why it is a consensus that  $\lambda$  must be a parameter sufficiently close to 1. In general,  $U({}^{(3)}g_{ij}, N)$  can depend on the spatial metric and the lapse function because of the symmetry of the theory. It is obvious that there are several invariant terms that one could include in  $U$ . Particular choices resulted in different versions of Hořava-Lifshitz gravity.

Motivated by condensed matter systems, P. Hořava proposed a symmetry on  $U$  that substantially reduces the number of invariants[17]. In this case,  $U$  depends on a superpotential  $W$  given by the Chern-Simons term, the curvature scalar and a term which mimics the cosmological constant. It has been shown [20] that this original assumption has to be broken if one intends to build a theory in agreement to current observations.

The simplification  $N = N(t)$  was also originally proposed by Hořava[17]. This condition defines a version of Hořava-Lifshitz gravity called Projectable. As  $\partial N / \partial x^i \equiv 0$ , the Projectable version also reduces the number of invariants that one can include in  $U$ . The linearization of this version assuming a Minkowski background provides an extra scalar degree of freedom which is classically unstable in the IR when  $\lambda > 1$  or  $\lambda < 1/3$ , and is a ghost when  $1/3 < \lambda < 1$  [21]. Although some physicists argue that higher order derivatives can cut off these instabilities, it has been shown[20, 23–25] that a perturbative analysis is not consistent when  $\lambda \rightarrow 1$  and the scalar mode gets strongly coupled. That is because the strongly coupled scale is unacceptably low. In this case, higher order operators would modify the graviton dynamics at very low energies, being in conflict with current observations.

Besides pure curvature invariants of  ${}^{(3)}g_{ij}$ , one may also include invariant contractions of  $a_i \equiv \partial(\ln N) / \partial x^i$  in  $U$ . This assumption defines the so-called Non-Projectable version of Hořava-Lifshitz gravity. Connected to the lowest order invariant  $a_i a^i$ , there is a parameter  $\sigma$  which defines a “safe” domain of the theory[21, 26]. In fact, in this case there is also an extra scalar degree of freedom when one linearizes the theory in a Minkowski background. However, when  $0 < \sigma < 2$  and  $\lambda > 1$  this mode is not a ghost nor classically unstable (as long as detailed balance is not imposed). Although the Non-Projectable version also exhibits a strong coupling[20, 26, 28], it has been argued that its scale is too high to be phenomenologically accessible from gravitational experiments[21].

In this paper we adhere to a particular version of Non-Projectable Hořava-Lifshitz gravity, in which the potential  $U_{\text{HL}}$  is given by

$$U_{\text{HL}} = \sigma a_i a^i + \alpha_{21} {}^{(3)}R^2 + \alpha_{22} {}^{(3)}R_j^i {}^{(3)}R_i^j + \alpha_{31} {}^{(3)}R^3 + \alpha_{32} {}^{(3)}R {}^{(3)}R_j^i {}^{(3)}R_i^j + \alpha_{33} {}^{(3)}R_j^i {}^{(3)}R_k^j {}^{(3)}R_i^k, \quad (5)$$

where  ${}^{(3)}R_{ij}$  is the spatial Ricci tensor and  $\alpha_{ij}$  are coupling constants. To complete the above Hořava-Lifshitz

action we add the remaining action

$$S \propto \int N \sqrt{{}^{(3)}g} [-2\Lambda - 2\mathcal{L}_m] d^3x dt, \quad (6)$$

with a cosmological constant  $\Lambda$  and where  $\mathcal{L}_m$  is the Lagrangean density of the matter content of the model, which we take as dust and radiation.

In the next section we analyze the structure of the phase space of a nonsingular Bianchi IX cosmological model with three scale factors – sourced with dust, radiation and a cosmological constant – which arises from Non-Projectable Hořava-Lifshitz gravity.

A similar model was previously considered by Misoh, Maeda and Kobayashi [22] and analyzed numerically. However their work did not contemplate the full Hamiltonian formulation of the phase space of the system and its basic and fundamental structures that organize the dynamics in the whole phase space. The connection of the authors' results with ours are discussed in the paper. For future reference we mention here that the parameters of the potential  $\mathcal{V}_{HL}$  used in [22], eq. (2.6), are related to the corresponding parameters of our paper according to

$$\begin{aligned} g_2 &= \alpha_{31}, & g_3 &= \alpha_{22}, \\ g_5 &= \alpha_{31}, & g_6 &= \alpha_{32}, & g_7 &= \alpha_{33}. \end{aligned}$$

The choice  $g_1 = -1$  in [22] is equivalent to include  ${}^{(3)}R$  in the expression  $(K_{ij}K^{ij} - \lambda K^2 - {}^{(3)}R)$  of eq. (4) of our paper; for  $\lambda = 1$  this expression constitutes the gravitational action of GR in the ADM formalism. The parameter  $g_8$  multiplies an expression that is zero in the case of the spatially homogeneous Bianchi IX metric; therefore this term was not included in  $U_{HL}$ , eq. (5) above. Concerning  $g_4$  and  $g_9$  we did not consider  $HL$  potential terms containing covariant spatial derivatives of the 3-dim Ricci tensor  ${}^{(3)}R_{ij}$ . The non-canonical variables  $(a, \beta_+, \beta_-)$  of [22] are related to the canonical variables  $(x, y, z)$ , defined in Section IV, by

$$a = 2x, \quad \beta_+ = (\ln z)/6, \quad \beta_- = \sqrt{3} (\ln y)/6.$$

## II. THE MODEL

The fundamental symmetry assumed in Hořava-Lifshitz gravity provides enough gauge freedom to choose

$$N = N(t), \quad N_i = 0. \quad (7)$$

Let us then consider a general Bianchi IX spatially homogeneous geometry with three scale factors in comoving coordinates,

$$ds^2 = N^2 dt^2 + h_{ij} \omega^i \omega^j \quad (8)$$

where  $t$  is the cosmological time and

$$\begin{aligned} h_{ij} &= \text{diag}(-M^2, -Q^2, -R^2), \\ h^{ij} &= \text{diag}\left(-\frac{1}{M^2}, -\frac{1}{Q^2}, -\frac{1}{R^2}\right). \end{aligned} \quad (9)$$

$(M(t), Q(t), R(t))$  are the scale factors of the model in the Bianchi IX 1-form basis  $\omega^i$  ( $i = 1, 2, 3$ ) which satisfy

$$d\omega^i = \frac{1}{2} \epsilon^{ijk} \omega^j \wedge \omega^k, \quad (10)$$

where  $d$  denotes the exterior derivative. In the basis  $\omega^i$  we have

$$K_{ij} = -\frac{1}{N} \dot{h}_{ij} = \frac{1}{N} (-M\dot{M}, -Q\dot{Q}, -R\dot{R}),$$

and

$$K^{ij} = -\frac{1}{N} \dot{h}^{ij} = \frac{1}{N} \left(-\frac{\dot{M}}{M^3}, -\frac{\dot{Q}}{Q^3}, -\frac{\dot{R}}{R^3}\right), \quad (11)$$

For future reference the nonvanishing spatial components of  ${}^{(3)}R^i_j$  are given by

$$\begin{aligned} {}^{(3)}R^1_1 &= -\frac{1}{M^2} + \frac{1}{2} \left[ -\frac{M^2}{Q^2 R^2} + \frac{Q^2}{M^2 R^2} + \frac{R^2}{M^2 Q^2} \right] \\ {}^{(3)}R^2_2 &= -\frac{1}{Q^2} + \frac{1}{2} \left[ \frac{M^2}{Q^2 R^2} - \frac{Q^2}{M^2 R^2} + \frac{R^2}{M^2 Q^2} \right] \\ {}^{(3)}R^3_3 &= -\frac{1}{R^2} + \frac{1}{2} \left[ \frac{M^2}{Q^2 R^2} + \frac{Q^2}{M^2 R^2} - \frac{R^2}{M^2 Q^2} \right] \end{aligned}$$

so that

$${}^{(3)}R = \frac{1}{2M^2 Q^2 R^2} [M^4 + Q^4 + R^4 - (R^2 - Q^2)^2 - (R^2 - M^2)^2 - (M^2 - Q^2)^2], \quad (12)$$

$$\begin{aligned} {}^{(3)}R^i_j {}^{(3)}R^j_i &= \frac{1}{4(MQR)^4} [3M^8 - 4M^6(Q^2 + R^2) \\ &\quad - 4M^2(Q^2 - R^2)^2(Q^2 + R^2) + 2M^4(Q^2 + R^2)^2 \\ &\quad + (Q^2 - R^2)^2(3Q^4 + 2Q^2 R^2 + 3R^4)], \end{aligned} \quad (13)$$

and

$$\begin{aligned} {}^{(3)}R^i_j {}^{(3)}R^j_k {}^{(3)}R^k_i &= \frac{1}{8(MQR)^6} \{ [(M^2 - Q^2)^2 - R^4]^3 \\ &\quad + [(M^2 - R^2)^2 - Q^4]^3 + [(Q^2 - R^2)^2 - M^4]^3 \}, \end{aligned} \quad (14)$$

which are the key terms to evaluate the potential  $U_{HL}$ . Therefore, Lagrangian of the total action resulting from (4)-(6) is given, up to a constant volume integral, by

$$\mathcal{L} \propto K - V$$

where the kinetic part  $K$  is given by

$$\begin{aligned} K &= \frac{MQR}{N} \left[ (1 - \lambda) \left( \frac{\dot{M}^2}{M^2} + \frac{\dot{Q}^2}{Q^2} + \frac{\dot{R}^2}{R^2} \right) \right. \\ &\quad \left. - 2\lambda \left( \frac{\dot{M}\dot{Q}}{MQ} + \frac{\dot{Q}\dot{R}}{QR} + \frac{\dot{M}\dot{R}}{MR} \right) \right], \end{aligned} \quad (15)$$

and the potential part  $V$  is

$$V = -N(MQR) \left[ {}^{(3)}R + 2\Lambda + U_{\text{HL}} + 2 \left( E_0 + \frac{E_r}{(MQR)^{1/3}} \right) \right], \quad (16)$$

where  $E_0$  and  $E_r$  are constants, corresponding to the separately conserved total energy of dust and radiation, respectively.  $U_{\text{HL}}$  was fixed in (5).

By defining then the canonical momenta as

$$p_M = \frac{\partial \mathcal{L}}{\partial \dot{M}}, \quad p_Q = \frac{\partial \mathcal{L}}{\partial \dot{Q}}, \quad p_R = \frac{\partial \mathcal{L}}{\partial \dot{R}}, \quad (17)$$

the total action can be reexpressed as

$$S \propto \int \left( \sum_i \dot{q}_i p_i - N\mathcal{H} \right) dt \quad (18)$$

so that  $\delta S/\delta N = 0$  results in the first integral of motion, the conserved Hamiltonian constraint

$$\begin{aligned} \mathcal{H} = & \frac{1}{4(3\lambda - 1)} \left[ (2\lambda - 1) \left( \frac{Mp_M^2}{QR} + \frac{Qp_Q^2}{MR} + \frac{Rp_R^2}{MQ} \right) \right. \\ & \left. - 2\lambda \left( \frac{p_M p_Q}{R} + \frac{p_M p_R}{Q} + \frac{p_Q p_R}{M} \right) \right] + 2\Lambda MQR \\ & + 2E_0 + \frac{2E_r}{(MQR)^{\frac{1}{3}}} + MQR[{}^{(3)}R + U_{\text{HL}}] = 0. \quad (19) \end{aligned}$$

From the point of view of dynamical systems we may consider  $E_0$  in (19) as the total conserved energy of the Hamiltonian dynamics so that we will refer to it as the total energy of the system. We also assume a positive cosmological constant  $\Lambda > 0$ .

From (19) we derive the equations of motion

$$\begin{aligned} \dot{M} &= \frac{(1 - 2\lambda)Mp_M + \lambda(Qp_Q + Rp_R)}{2QR(1 - 3\lambda)} \\ \dot{Q} &= \frac{(1 - 2\lambda)Qp_Q + \lambda(Mp_M + Rp_R)}{2MR(1 - 3\lambda)} \\ \dot{R} &= \frac{(1 - 2\lambda)Rp_R + \lambda(Mp_M + Qp_Q)}{2QM(1 - 3\lambda)} \\ \dot{p}_M &= \frac{(1 - 2\lambda)[M^2p_M^2 + Q^2p_Q^2 + R^2p_R^2] - 2\lambda QRp_Qp_R}{4(3\lambda - 1)M^2QR} - \Lambda QR + \frac{QRE_r}{3(MQR)^{\frac{4}{3}}} \\ &+ QR[{}^{(3)}R + U] + MQR \frac{\partial}{\partial M} [{}^{(3)}R + U_{\text{HL}}] \\ \dot{p}_Q &= \frac{(1 - 2\lambda)[M^2p_M^2 + Q^2p_Q^2 + R^2p_R^2] - 2\lambda MRp_Mp_R}{4(3\lambda - 1)MQ^2R} - \Lambda MR + \frac{MRE_r}{3(MQR)^{\frac{4}{3}}} \\ &+ MR[{}^{(3)}R + U] + MQR \frac{\partial}{\partial Q} [{}^{(3)}R + U_{\text{HL}}] \\ \dot{p}_R &= \frac{(1 - 2\lambda)[M^2p_M^2 + Q^2p_Q^2 + R^2p_R^2] - 2\lambda MQp_Mp_Q}{4(3\lambda - 1)MQR^2} - \Lambda MQ + \frac{MQE_r}{3(MQR)^{\frac{4}{3}}} \\ &+ MQ[{}^{(3)}R + U] + MQR \frac{\partial}{\partial R} [{}^{(3)}R + U_{\text{HL}}]. \end{aligned} \quad (20)$$

The above equations were derived for the most general case in which  $\lambda$  is an additional free parameter of the model. From a dynamical system point of view, this would be interesting in order to study the role of  $\lambda$  in the phase space dynamics. However, in order to recover General Relativity in the IR, not only  $\sigma \rightarrow 0$ , but also  $\lambda \rightarrow 1$  [21]. In fact, in the framework of Hořava-Lifshitz,  $\lambda$  must be sufficiently close to 1 in order to guarantee that no serious Lorentz invariance violation occurs. Therefore, in order to simplify our analysis, in the remaining of the paper we will be restricted to the case  $\lambda = 1$ .

### III. THE SKELETON OF THE PHASE SPACE

In order to have an overall view of the phase space of the system, in the present section we will examine the basic structures that organize the dynamics of the phase space. The first of these is the invariant plane defined by

$$p_M = p_Q = p_R, \quad M = Q = R, \quad (21)$$

so that the Hamiltonian (19) for the dynamics in the invariant plane reduces to

$$\mathcal{H}_I = \frac{3}{8} \frac{p_M^2}{M} + V(M) - 2E_0 = 0. \quad (22)$$

where

$$V(M) = \frac{3}{2}M - 2\Lambda M^3 - \frac{A_2}{M} + \frac{A_3}{M^3}, \quad (23)$$

$$A_2 = 3\alpha_{21} + \alpha_{22} + \frac{8E_r}{3}, \quad (24)$$

$$A_3 = 9\alpha_{31} + 3\alpha_{32} + \alpha_{33}. \quad (25)$$

From the expression of  $V(M)$  we see that the bounce condition implies  $A_3 > 0$ , so that we will restrict ourselves to this case in the paper, corresponding to a well-behaved dynamics. Furthermore in order to have a deSitter attractor at infinity, corresponding to a possible exponentially expanding phase for orbits of the system, we will fix  $\Lambda > 0$ .

The critical points of the phase space are defined as equilibrium points of the dynamics (20), and given by

$$p_M = p_Q = p_R = 0, \quad M = Q = R = M_0, \quad (26)$$

where  $M_0$  is a positive constant satisfying

$$M_0^6 - \frac{M_0^4}{4\Lambda} - \frac{A_2 M_0^2}{8\Lambda} + \frac{3A_3}{16\Lambda} = 0, \quad (27)$$

so that the right-hand-side of (20) vanishes. Obviously the critical points belong to the invariant plane. From (22) we obtain that the energy of a critical point  $M_0$  is given by

$$E_{cr} = \frac{3}{4}M_0 - \Lambda M_0^3 + \frac{3}{16} \frac{A_3}{M_0^3} - \frac{3}{8} \frac{A_2}{M_0}. \quad (28)$$

By fixing  $A_3 > 0$  and  $\Lambda > 0$  as postulated above, a careful analysis of (27) shows that we have at most two critical points, or one critical point or no critical point depending on the values of  $\Lambda$ ,  $A_2$  and  $A_3$ . Each critical point corresponds to a real positive root of (27) with  $E_{cr} > 0$  in (28).

Figure 1 illustrates the invariant plane and the critical points in the finite region of the phase space for the parameters  $\Lambda = 1$ ,  $A_2 = 0.05$  and  $A_3 = 0.005$ . The graph is made in the canonical variables  $(x, p_x)$  of the invariant plane to be introduced in Section IV. In these coordinates the critical points are given by  $P_1 = (0.2348551826828089, 0)$  and  $P_2 = (0.51007113736321, 0)$ . Dashed and dotted orbits shown in the invariant plane correspond to the energies  $E_0 = 0.250$ , and  $E_0 = 0.185$ , respectively. The energy of the critical point  $P_2$  is  $E_0 = 0.2201517192605279$  and corresponds also to the separatrix (solid line) which is homoclinic connection of  $P_2$  to itself. The separatrix divides the invariant plane into three disconnected regions: region (I), of bounded periodic orbits corresponding to eternal oscillating universe, and regions (II) and (III) of one-bounce universes emerging from the deSitter repeller and tending to a deSitter attractor at infinity. The scale factor approaches the deSitter asymptotic configurations as  $x \sim \exp(t\sqrt{\Lambda/3})$  and  $p_x \sim \exp(t\sqrt{4\Lambda/3})$  for times going to  $\pm\infty$ . As will be shown along the paper

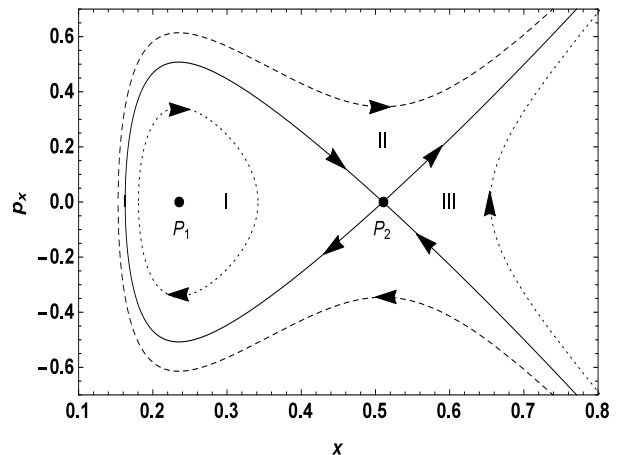


FIG. 1: The invariant plane. Here we fixed the parameters  $\Lambda = 1$ ,  $A_2 = 0.05$  and  $A_3 = 0.005$ . Dashed, solid and dotted lines correspond to  $E_0 = 0.250$ ,  $E_0 = 0.2201517192605279$  and  $E_0 = 0.185$ , respectively. The second value of the energy is the energy of the critical point  $P_2$ , and the solid line constitutes a homoclinic connection of  $P_2$  to itself. The critical points are given by  $P_1 = (0.2348551826828089, 0)$  and  $P_2 = (0.51007113736321, 0)$ . The graph was made in the canonical variables  $(x, p_x)$  introduced in Section IV.

some parametric configurations may also present velocity dominated attractors at infinity.

Finally we should mention that the phase space of the dynamical system (20) presents two invariant submanifolds defined by

$$M = Q, \quad p_M = p_Q, \quad (29)$$

and

$$Q = R, \quad p_Q = p_R. \quad (30)$$

The denomination invariant submanifolds derives from the fact that each of them is mapped into itself by the general Hamiltonian flow (20), in other words, is invariant under the flow. In particular the invariant plane (21) corresponds to the intersection of these two submanifolds and satisfies obviously this property.

The nature of the critical points is characterized by linearizing the dynamical equations (20) about the critical point. Defining

$$X = (M - M_0), \quad W = (p_M - 0), \quad (31)$$

$$Y = (Q - M_0), \quad K = (p_Q - 0), \quad (32)$$

$$Z = (R - M_0), \quad L = (p_R - 0), \quad (33)$$

small, we obtain from (20)

$$\begin{pmatrix} \dot{X} \\ \dot{Y} \\ \dot{Z} \\ \dot{W} \\ \dot{K} \\ \dot{L} \end{pmatrix} = \begin{pmatrix} 0 & 0 & 0 & \alpha & -\alpha & -\alpha \\ 0 & 0 & 0 & -\alpha & \alpha & -\alpha \\ 0 & 0 & 0 & -\alpha & -\alpha & \alpha \\ \delta & \gamma & \gamma & 0 & 0 & 0 \\ \gamma & \delta & \gamma & 0 & 0 & 0 \\ \gamma & \gamma & \delta & 0 & 0 & 0 \end{pmatrix} \begin{pmatrix} X \\ Y \\ Z \\ W \\ K \\ L \end{pmatrix} \quad (34)$$

where

$$\alpha = \frac{1}{4M_0}, \quad (35)$$

$$\delta = \frac{1}{M_0^3} \left( -\frac{8E_r}{9} - 3\alpha_{22} + 7\alpha_{21} \right) - \frac{3}{M_0} + \frac{1}{4M_0^5} (27\alpha_{33} - 45\alpha_{31} + 17\alpha_{32}), \quad (36)$$

$$\gamma = \frac{1}{4M_0^3} \left( -\frac{8E_r}{9} + 5\alpha_{22} - 17\alpha_{21} \right) + \frac{3}{2M_0} + \frac{1}{8M_0^5} (-21\alpha_{33} + 99\alpha_{31} + \alpha_{32}) - 2\Lambda M_0. \quad (37)$$

The nature of a critical points  $M_0$  is determined by the characteristic polynomial associated with the linearization matrix in (34). We obtain

$$P(L) = (L - L_1)(L + L_1)(L - L_2)^2(L + L_2)^2, \quad (38)$$

with roots

$$L_1 = \pm \sqrt{-\alpha(2\gamma + \delta)}, \quad L_2 = \pm \sqrt{2\alpha(\delta - \gamma)}, \quad (39)$$

where the second pair has multiplicity two.

We see that the characterization of the critical points  $M_0$  and of the structure of the phase in its neighborhood of the critical points is highly complex, depending on the domains of the parameters appearing in the Hamiltonian (19).

With view to a numerical illustration we give here  $L_1$  and  $L_2$  in terms of the parameters,

$$L_1 = \pm \frac{1}{2\sqrt{2}} \sqrt{8\Lambda + \frac{A_2}{M_0^4} - \frac{3A_3}{M_0^6}}, \quad (40)$$

$$L_2 = \pm \frac{\sqrt{2}}{4M_0^3\sqrt{3}} \left( \frac{225}{2}A_3 - 144(9\alpha_{31} + 2\alpha_{32}) - M_0^2 \times (51A_2 + 54M_0^2 - 128E_r - 288\alpha_{21} - 24\Lambda M_0^4) \right)^{1/2}, \quad (41)$$

with  $L_2$  having multiplicity 2. As we are restricting ourselves to the case of two critical points, namely  $\Lambda > 0$  and  $A_3 > 0$ , four main configurations are present. Let  $P_1$  and  $P_2$  denote the two critical points in the invariant plane. The following possible configurations are then:

(A)  $P_1$  is a center-center-center and  $P_2$  is a saddle-center-center;

(B)  $P_1$  is a center-saddle-saddle and  $P_2$  is a saddle-center-center;

(C)  $P_1$  is a center-saddle-saddle and  $P_2$  is a saddle-saddle-saddle;

(D)  $P_1$  is a center-center-center and  $P_2$  is a saddle-saddle-saddle.

In the above we must remark that the denomination ‘‘center-center-center’’ actually denotes the topology of a center times a center with multiplicity 2, and ‘‘saddle-saddle-saddle’’ denotes the topology of a saddle times a saddle with multiplicity 2, and so on.

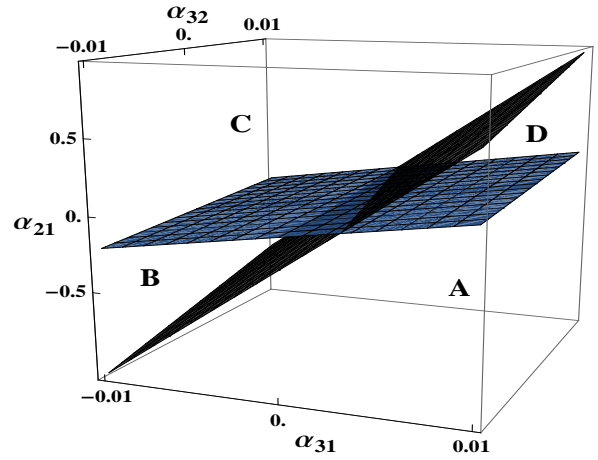


FIG. 2: The parameter space  $(\alpha_{31}, \alpha_{32}, \alpha_{21})$  and the four 3-dim domains corresponding to the configurations (A), (B), (C) and (D) of the critical points.

For an illustration of the parameter domains corresponding to such configurations let us fix  $A_2 = 0.05$ ,  $A_3 = 0.005$  and  $\Lambda = 1$ . Furthermore, we will also fix  $E_r = 0.1$ . We obtain for the four configurations:

(A)  $P_1$  is a center-center-center and  $P_2$  is a saddle-center-center:  $\alpha_{21} < -0.0609122 + 81.5854\alpha_{31} + 18.1301\alpha_{32}$  and  $\alpha_{21} < 0.0000442278 + 17.2962\alpha_{31} + 3.8436\alpha_{32}$ ,

(B)  $P_1$  is a center-saddle-saddle and  $P_2$  is a saddle-center-center:  $\alpha_{21} > -0.0609122 + 81.5854\alpha_{31} + 18.1301\alpha_{32}$  and  $\alpha_{21} < 0.0000442278 + 17.2962\alpha_{31} + 3.8436\alpha_{32}$ ,

(C)  $P_1$  is a center-saddle-saddle and  $P_2$  is a saddle-saddle-saddle:  $\alpha_{21} > -0.0609122 + 81.5854\alpha_{31} + 18.1301\alpha_{32}$  and  $\alpha_{21} > 0.0000442278 + 17.2962\alpha_{31} + 3.8436\alpha_{32}$ ,

(D)  $P_1$  is a center-center-center and  $P_2$  is a saddle-saddle-saddle:  $\alpha_{21} < -0.0609122 + 81.5854\alpha_{31} + 18.1301\alpha_{32}$  and  $\alpha_{21} > 0.0000442278 + 17.2962\alpha_{31} + 3.8436\alpha_{32}$ ,

which are illustrated in Fig. 2. We must observe that the domains (A), (B), (C) and (D) do not overlap by definition, and consequently the shaded surfaces shown in Fig. 2 do not belong to any of the four domains.

As we will see the high instability of the dynamics in the cases (B) – (D) is connected with the presence of saddles with multiplicity two, discussed in the following sections.

#### IV. THE DYNAMICS ABOUT THE CRITICAL POINTS: THE CASE OF A CENTER-CENTER-CENTER AND A SADDLE-CENTER-CENTER

We now describe the topology and the invariant manifolds of the dynamics in the linear neighborhood of the critical points. We will then apply this analysis to the parameter domain (A), corresponding the case of a center-center-center  $P_1$  and a saddle-center-center  $P_2$ . To start let us introduce the canonical transformation with the generating function

$$G = (MQR)^{1/3}p_x + \frac{M}{Q}p_y + \frac{MQ}{R^2}p_z, \quad (42)$$

where  $p_x$ ,  $p_y$  and  $p_z$  are the new momenta, resulting in

$$x = (MQR)^{1/3}, \quad y = \frac{M}{Q}, \quad z = \frac{MQ}{R^2}, \quad (43)$$

and

$$\begin{aligned} p_M &= \frac{1}{3} \frac{QR}{(MQR)^{2/3}} p_x + \frac{1}{Q} p_y + \frac{Q}{R^2} p_z, \\ p_Q &= \frac{1}{3} \frac{MR}{(MQR)^{2/3}} p_x - \frac{M}{Q^2} p_y + \frac{M}{R^2} p_z, \\ p_R &= \frac{1}{3} \frac{MQ}{(MQR)^{2/3}} p_x - \frac{2MQ}{R^3} p_z. \end{aligned} \quad (44)$$

Here, the variable  $x$  is obviously the average scale factor of the model. In these new canonical variables the equations of the invariant plane reduce to

$$y = 1, \quad z = 1, \quad p_y = 0 = p_z. \quad (45)$$

The new variables  $(x, p_x)$  are then seen to be defined on the invariant plane. These variables were used in constructing Fig. 1 displaying the invariant plane in the parameter domain (A).

In the new variables  $(x, p_x, y, p_y, z, p_z)$  the full Hamiltonian (19) assumes the form

$$\begin{aligned} \mathcal{H} &= -\frac{p_x^2}{24x} + \frac{p_y^2 y^2}{2x^3} + \frac{3p_z^2 z^2}{2x^3} + \frac{x}{2z^{4/3}} - \frac{x}{yz^{1/3}} - \frac{xy}{z^{1/3}} \\ &- xz^{2/3} + \frac{xz^{2/3}}{2y^2} + \frac{1}{2}xy^2z^{2/3} + 2x^3\Lambda + 2E_0 + \frac{2E_r}{x} \\ &+ x^3U_{HL}(x, y, z) = 0 \end{aligned} \quad (46)$$

These new canonical variables are very useful since they separate the degrees of freedom of the system about the critical points into the expansion/contraction mode  $(x, p_x)$ , connected to the invariant plane, and the modes  $(y, p_y)$  and  $(z, p_z)$  that – in the case of a center-center-center or a saddle-center-center – are pure rotational modes about the critical point. These variables allow us to describe the topology of the general dynamics in a linear neighborhood of the critical points as well as to

examine the nonlinear extension of invariant manifolds about the critical points as we proceed to show.

To see this we expand the Hamiltonian (46) in a linear neighborhood of the critical point  $(x = M_0, p_x = 0, y = 1, p_y = 0, z = 1, p_z = 0)$ , resulting in the quadratic form

$$\begin{aligned} \mathcal{H}_L &= 2(E_0 - E_{cr}) - \left[ \frac{p_x^2}{24M_0} - q_x(x - M_0)^2 \right] \\ &+ \left[ \frac{1}{2} \frac{p_y^2}{M_0^3} + 3q(y - 1)^2 \right] \\ &+ \left[ \frac{3}{2} \frac{p_z^2}{M_0^3} + q(z - 1)^2 \right] = 0, \end{aligned} \quad (47)$$

where

$$\begin{aligned} q_x &= 6\Lambda M_0 + \frac{1}{4M_0^3}(3\alpha_{22} + 9\alpha_{21} + 8E_r) \\ &- \frac{1}{4M_0^5}(9\alpha_{33} + 27\alpha_{32} + 81\alpha_{31}), \end{aligned} \quad (48)$$

$$\begin{aligned} q &= \frac{1}{4M_0^3}(9\alpha_{31} - \alpha_{32} - 3\alpha_{33}) \\ &+ \frac{1}{3M_0}(\alpha_{22} - 3\alpha_{21}) + \frac{M_0}{3}. \end{aligned} \quad (49)$$

In deriving (47) the equations defining the critical points (27) and their respective energy (28) were used. At this point it is worth mentioning that, in terms of the parameters  $q_x$  and  $q$ , the four parametric domain configurations given in the previous section can be simply characterized as

- (A)  $P_1 : (q_x < 0, q > 0), \quad P_2 : (q_x > 0, q > 0),$
- (B)  $P_1 : (q_x < 0, q < 0), \quad P_2 : (q_x > 0, q > 0),$
- (C)  $P_1 : (q_x < 0, q < 0), \quad P_2 : (q_x > 0, q < 0),$
- (D)  $P_1 : (q_x < 0, q > 0), \quad P_2 : (q_x > 0, q < 0).$

The quadratic Hamiltonian (47) is obviously separable and can be reexpressed as

$$\mathcal{H}_L = 2(E_{cr} - E_0) + E_x - E_1 - E_2 = 0 \quad (50)$$

where

$$E_x = \frac{p_x^2}{24M_0} - q_x(x - M_0)^2, \quad (51)$$

$$E_1 = \frac{1}{2} \frac{p_y^2}{M_0^3} + 3q(y - 1)^2, \quad (52)$$

$$E_2 = \frac{3}{2} \frac{p_z^2}{M_0^3} + q(z - 1)^2, \quad (53)$$

are constants of motion of the linearized motion about the critical point  $M_0$  in the sense that they have zero Poisson brackets with the Hamiltonian  $\mathcal{H}_L$ . Two additional constants of the linearized motion are also present,

$$C_1 = \left( \frac{1}{2M_0^3} p_y p_z + q YZ \right), \quad (54)$$

$$C_2 = \left( Y p_z - \frac{1}{3} Z p_y \right), \quad (55)$$

where in the above  $Y \equiv (y - 1)$  and  $Z \equiv (z - 1)$ . They are not all independent but related by

$$4E_1E_2 = 12C_1^2 + 6C_2^2. \quad (56)$$

We introduce a third constant of motion defined by

$$C_3 = (E_1 - E_2), \quad (57)$$

that together with  $C_1$  and  $C_2$  satisfy the algebra

$$\begin{aligned} [C_1, C_2] &= -\frac{1}{3} C_3, & [C_2, C_3] &= -4 C_1, \\ [C_3, C_1] &= -\frac{6q}{M_0^3} C_2. \end{aligned} \quad (58)$$

We are now ready to describe the topology of the 6-dim phase space in the linear neighborhood of the critical points. In the remaining of this section we will restrict ourselves to the parameter domain (A) for which both critical points  $P_1$  and  $P_2$  have  $q > 0$ , cf. (49).

Let us consider the case  $E_x = 0$  corresponding to  $(x = M_0, p_x = 0)$ . The motion about the critical points in this case are periodic orbits of the isotropic harmonic oscillator

$$\mathcal{H}_L = E_1 + E_2 = 2(E_0 - E_{cr}). \quad (59)$$

In fact, by a proper canonical rescaling of the variables in (59), we can show that these energy surfaces are hyperspheres and that the group generated by the constants of motion (54), (55) and (57) is homomorphic to the unitary unimodular group with the topology of  $S^3$ [36, 37]. These energy surfaces are denoted the center manifold  $S^3$  of unstable periodic orbits, a structure that extends to the nonlinear phase space domain about the critical points.

Now due to the separate conservation of  $E_1$  and  $E_2$  in (59) we can show that the center manifold in the linear neighborhood of the critical points is foliated by Clifford 2-dim surfaces in  $S^3$ [38], namely, 2-tori  $\mathcal{T}_{E_0}$  contained in the energy surface  $E_0 = \text{const}$ . The Clifford surfaces as well as the  $S^3$  manifold containing them depend continuously on the parameter  $E_0$ . These two tori will have limiting configurations which are periodic orbits, whenever  $E_1 = 0$  or  $E_2 = 0$ .

From equation (59) we have that  $(E_0 - E_{cr}) < 0$  is a necessary condition for the dynamics in the rotational sector (59), defining a condition for the existence of the center manifold  $S_{E_0}^3$  of periodic orbits. For  $E_0 = E_{cr}$  the center manifold reduces to the critical point. By continuity as  $(E_{cr} - E_0)$  increases the nonlinear extension of the center manifold maintains the topology of  $S^3$  but will no longer be decomposable into  $E_1$  and  $E_2$ . A detailed description of the center manifold and its nonlinear extension will be the object of the next Section.

The second possibility to be considered is the motion in the sector  $(x, p_x)$ . In the parameter domain (A) the case of  $E_x$  demands a separate analysis for the two critical

points, since we have  $q_x > 0$  for the critical point  $P_2$  so that  $E_x$  corresponds to the energy associated with the motion in the saddle sector. We remind that this is related to the fact that the pair of eigenvalues (40) are real for  $P_2$ .

We should remark that for the critical point  $P_1$ , in which  $q_x < 0$ ,  $E_x$  is positive definite and corresponds to the rotational energy in the additional rotational sector  $(x, p_x)$  of the dynamics about  $P_1$  so that the general motion about  $P_1$  will have the topology  $S^1 \times S^3$ . All the orbits of the dynamics about  $P_1$  will be oscillatory corresponding to perpetually nonsingular bouncing universes.

In the following our focus will be in the phenomena connected to the saddle-center-center critical point  $P_2$  present in the phase space of the model. The general dynamics in the linear neighborhood of  $P_2$  is more complex and comes from the presence of the saddle sector associated with  $q_x > 0$ , as we discuss now.

If  $E_x = 0$  we have two possibilities. The first is  $(x = M_0, p_x = 0)$  which corresponds to the motion in the center-center ( $S^3$ ) sector already examined.

The second possibility is  $p_x = \pm\sqrt{24M_0q_x}(x - M_0)$  which defines the linear stable  $V_S$  and linear unstable  $V_U$  manifolds of the saddle sector.  $V_S$  and  $V_U$  limit regions *I* ( $E_x < 0$ ) and regions *II* ( $E_x > 0$ ) of motion on hyperbolae that are solutions of the separable saddle sector  $E_x = p_x^2/24M_0 - q_x(x - M_0)^2$ . Note that the saddle sector depicts the neighborhood of  $P_2$  in Figure 1, with  $V_S$  and  $V_U$  tangent to the separatrices at  $P_2$ . The direct product of  $\mathcal{T}_{E_0} \subset S^3$  with  $V_S$  and  $V_U$  generates, in the linear neighborhood of  $P_2$ , the structure of stable ( $\mathcal{T}_{E_0} \times V_S$ ) and unstable ( $\mathcal{T}_{E_0} \times V_U$ ) 3-dim surfaces that coalesce into the 2-dim tori  $\mathcal{T}_{E_0}$  for times going to  $+\infty$  and  $-\infty$  respectively. The energy on any orbit on these tubes is the same as that of the orbits on the tori  $\mathcal{T}_{E_0}$ .

These 3-dim tubes are contained in the 4-dim tubes which are respectively the product of  $V_S$  and  $V_U$  times the center manifold  $S_{E_0}^3$ , in the 5-dim energy surface  $\mathcal{H} = 0$  (46) with  $E_0 - E_{cr} < 0$ . They constitute a boundary for the general dynamical flow and are defined by  $E_x = 0$  in the linear neighborhood of  $P_2$ . Depending on the sign of  $E_x$  the motion will be confined inside the 4-dim tube (for  $E_x < 0$ ) and will correspond to a flow separated from the flow outside the tube (for  $E_x > 0$ ). The extension of structure of the 4-dim tubes away from the neighborhood of the center manifold  $S_{E_0}^3$  are now to be examined and our basic interest will reside in the stable and unstable pair,  $S_{E_0}^3 \times V_S$  and  $S_{E_0}^3 \times V_U$ , that leave the neighborhood of  $P_2$  towards the bounce.

In the two following sections the nature of the center-manifolds about critical points with a center-center sector and the typical phase space dynamics of the system are analyzed, for the parameter domain (A). The examination of some fundamental results are extended for general cases so that they can be applied in the remaining sections of the paper.

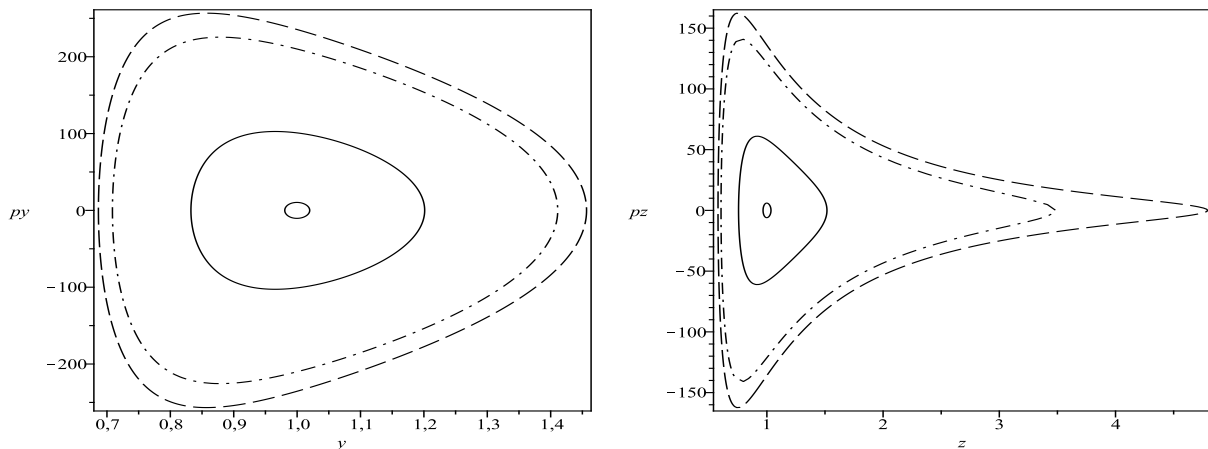


FIG. 3: Section  $p_z = 0, z = 1$  (left) and section  $p_y = 0, y = 1$  (right) of the center manifold  $S^3$  (60), for  $E_0 = 9.89, 9.0, 6.0, 5.0$ , about the critical point  $P_2$ , with parameters (61) in (A). The energy of  $P_2$  is  $E_{cr_2} = 9.89949505925050$ .

## V. THE CENTER MANIFOLD AND THE BOUNCING OSCILLATORY DYNAMICS

One of the main important uses of the canonical coordinates (42) is to give an exact analytical form of the center manifold as well as a sufficiently accurate numerical description of the phase space dynamics in extended regions away from the critical points. As we will see the center manifold is a fundamental structure connected with the whole oscillatory motion in the phase space.

We start by examining the nonlinear extension of the center manifold about the saddle-center-center critical point  $P_2$  restricted to the parametric domain (A) (the same analysis applies to the center manifold about the center-center-center critical point  $P_1$ ). In the canonical variables  $(y, z, p_y, p_z)$  the equation of the center manifold is obtained by substituting  $(x = x_{cr_2}, p_x = 0)$  in (46), yielding the exact expression

$$\begin{aligned} \mathcal{H}_C = & \frac{y^2 p_y^2}{2x_{cr_2}^3} + \frac{3z^2 p_z^2}{2x_{cr_2}^3} + \frac{x_{cr_2}}{2z^{4/3}} - \frac{x_{cr_2}}{yz^{1/3}} - \frac{x_{cr_2} y}{z^{1/3}} \\ & - x_{cr_2} z^{2/3} + \frac{x_{cr_2} z^{2/3}}{2y^2} + \frac{1}{2} x_{cr_2} y^2 z^{2/3} + 2x_{cr_2}^3 \Lambda \\ & + x_{cr_2}^3 U_{HL}(x_{cr_2}, y, z) + \frac{2E_r}{x_{cr_2}} + 2E_0 = 0, \quad (60) \end{aligned}$$

where  $x_{cr_2}$  is the average scale factor of the saddle-center-center critical point  $P_2$ . The domain of  $E_0$  defining the center manifold satisfies the constraint  $E_0 < E_{cr}$  as already discussed. For  $E_0 = E_{cr}$  the center manifold reduces to the critical point. In this section we are restricted to the parameter domain (A) and, for illustrative purposes, we will initially adopt the parameters

$$\begin{aligned} \Lambda &= 0.001, \quad Er = 10, \\ \alpha_{31} &= 10^{-4}, \quad \alpha_{32} = 10^{-5}, \quad \alpha_{33} = 0.00092, \quad (61) \\ \alpha_{21} &= -100, \quad \alpha_{22} = 580/3. \end{aligned}$$

For this parameter configuration the critical point  $P_2$  is given by  $(x_{cr_2} = 14.14213521493478, p_x = 0, y = 1, p_y = 0, z = 1, p_z = 0)$  with a corresponding critical energy  $E_{cr_2} = 9.89949505925050$ . The center manifold (60) is illustrated in Figures 3 where we display its sections ( $p_z = 0, z = 1$ ) and ( $p_y = 0, y = 1$ ) about  $P_2$  for several decreasing values of  $E_0 = 9.89, 9.0, 6.0, 5.0$ , illustrating the  $S^3$  topology of (60) and its deformation as the parameter  $(E_{cr} - E_0)$  increases.

The center manifold (60) is the locus of unstable periodic orbits or of oscillatory orbits of the system and organizes the finite phase space dynamics. In the case of the center manifold about the saddle-center-center  $P_2$ , let us consider for simplicity the section  $(y = 1, p_y = 0)$  of Figure 3 (right) for the energy  $E_0 = 9.8994$ . This section has the topology of  $S^1$  and is a solution of the constraint (60),  $\mathcal{H}_C(y = 1, p_y = 0, z, p_z, E_0) = 0$ , with  $(E_{cr} - E_0) \simeq 9.5 \times 10^{-5}$ . The points of this section are initial conditions for perpetually bouncing orbits, propagated forward or backward in time, as can be verified numerically. Let us take for instance the point  $(z = 1, p_z = 0.598741056178016)$  as initial conditions on  $S^1$ . The result of the dynamics is a perpetually bouncing universe illustrated in Figures 4. In Figure 4 (left) we can see that the orbit undergoes a long time oscillation on the center manifold – namely at  $(x = x_{cr} = 14.14213521493478, p_x = 0)$  – with short intervals of escaping from this neighborhood towards the bounces at  $x_b \simeq 4.565245$ , with a period between the bounces of  $\Delta t \simeq 855.975$ .

The oscillatory behavior of the modes  $(z, p_z)$  is illustrated in Figure 4 (right) showing long time oscillations about the center manifold with short intervals in which the orbit visits the bounce and returns again to the neighborhood of the center manifold. We note that the frequency of the mode  $p_z(t)$  increases substantially at the bounces. Analogous behavior is present in the variable  $z(t)$ , as expected. These patterns were verified for a long

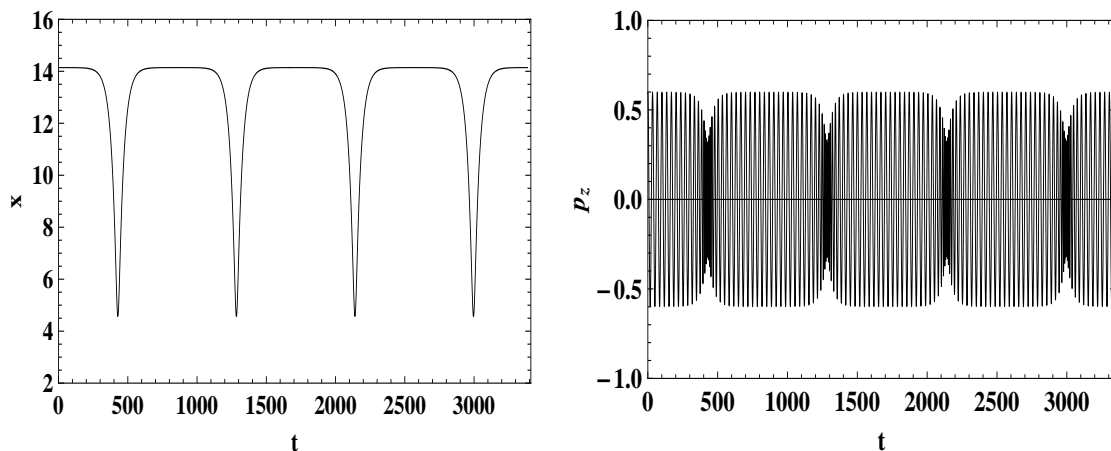


FIG. 4: (Left) The evolution of the scale factor  $x(t)$  for a periodic orbit having infinite bounces, with parameters (61) in (A) and initial conditions on a  $S^1$  section of the center manifold. (Right) The evolution of the oscillatory mode  $p_z(t)$ . We note that the frequency of the mode increases substantially as the orbit bounces.

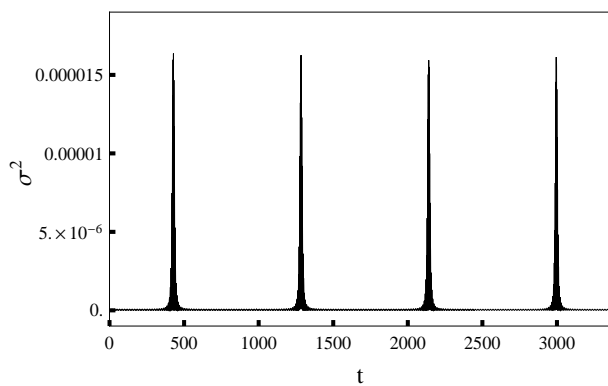


FIG. 5: Plot of the evolution of the anisotropy parameter  $\sigma^2$  related to the periodic orbit with infinite bounces displayed in Figs. 4, showing a relative large amplification in the oscillations when the orbit visits a neighborhood of the bounces.

time evolution. Actually in all our numerical treatment the Hamiltonian constraint (46) is conserved within a numerical error  $\leq 10^{-13}$  for the whole computational domain. These orbits constitute a set of perpetually bouncing periodic orbits present in the dynamics of the model.

Summarizing, as discussed already in the previous section, the orbits  $(x(t), p_x(t), y(t), p_y(t), z(t), p_z(t))$  emerge from the  $S^3$  center manifold towards the bounce generating the 4-dim stable and unstable cylinders  $R \times S^3$ , the motion along the cylinders being obviously oscillatory. For simplicity we restricted our numerical illustration to the motion in the invariant submanifold  $(y = 1, p_y = 0)$  with initial conditions taken on the 1-dim manifold  $S^1 \subset S^3$  defined by  $\mathcal{H}_C(y = 1, p_y = 0, z, p_z) = E_{cr} - E_0$  where  $E_0 = 9.8994$ , corresponding to an energy of rotational motion in the sector  $(z, p_z)$  of  $\simeq 1.52 \times 10^{-4}$ . In fact the orbits discussed above are strictly periodic bouncing orbits and therefore are not orbits homoclinic to the center manifold in which case they would take an infinite time

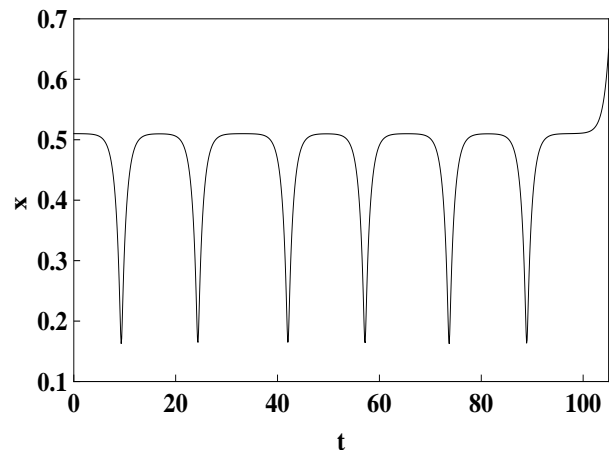


FIG. 6: The evolution of the scale factor  $x(t)$  for an orbit with parameters (63) in (A) exhibiting six bounces before the orbit escapes to the de Sitter attractor at infinity.

to its return to the center manifold.

Finally for future reference we will introduce a new quantity of the dynamics, the square of the shear tensor  $\sigma_{\alpha\beta}$  associated to the four velocity vector  $V^\alpha = \delta_0^\alpha$  of a comoving observer with the matter content of the model. In the coordinate system of the metric (8) for the gauge  $N = 1$  we obtain, after a straightforward calculation, that

$$\sigma^2 \equiv \frac{2}{3} \sigma^{\alpha\beta} \sigma_{\alpha\beta} = \frac{3(z p_z)^2 + (y p_y)^2}{3x^6}, \quad (62)$$

in the new canonical variables (42)-(44). We can see that  $\sigma^2$  – which is a measure of the anisotropy of the motion – is basically associated with the rotational modes of the system and has a smooth behavior. This is illustrated in Fig. 5 where we display  $\sigma^2$  versus  $t$  for the perpetually bouncing orbit of Figs. 4 in the parameter domain (A),

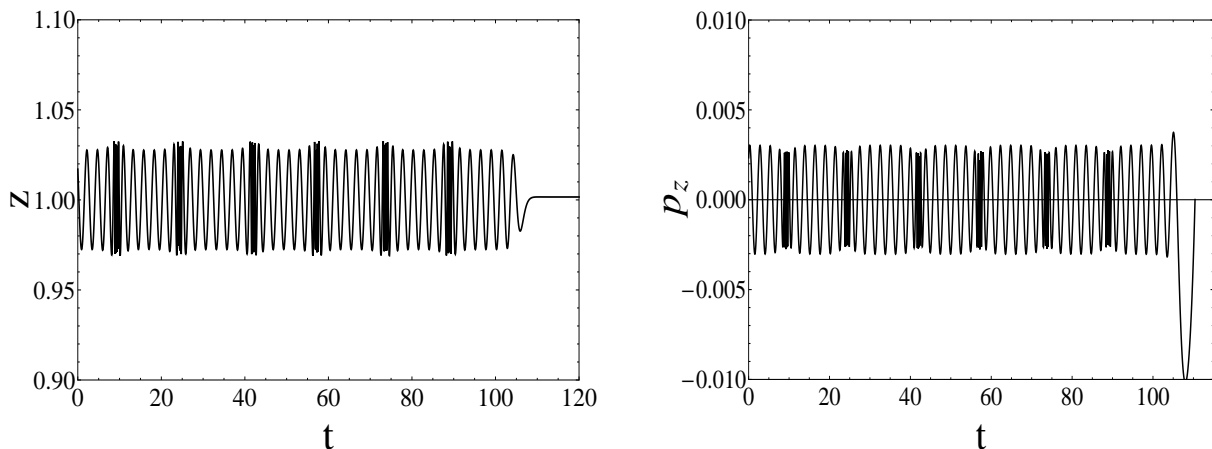


FIG. 7: The evolution of the oscillatory modes  $p_z(t)$  (left) and  $z(t)$  (right) of the orbit of Fig. 6. The frequency of the modes increases substantially in the neighborhood of the bounces. As the orbit approaches the de Sitter attractor the variables approach the constant values ( $z \sim 1, p_z \sim 0$ ) as expected.

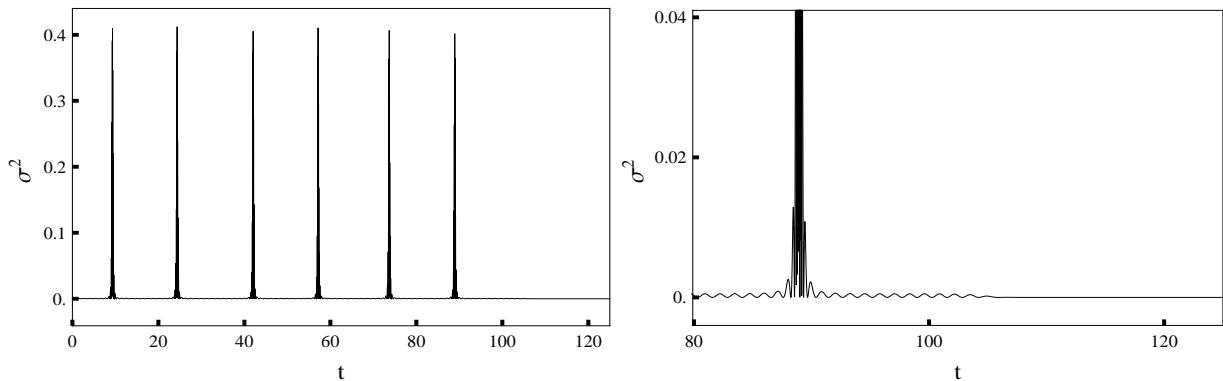


FIG. 8: (Left) Plot of the evolution of the shear parameter  $\sigma^2$  for the orbit of Figs. 6. (Right) Amplification of the final part of the signal showing that the shear becomes zero as the orbit reaches the de Sitter attractor.

showing a relatively large amplification as the orbit visits a neighborhood of the bounces.

On the other hand the parameter  $\sigma^2$  can play a role in the recognition and characterization of patterns in the phase space dynamics, connected to the presence of a saddle-saddle-saddle critical point. It will constitute an important numerical indicator of the existence of highly anisotropic momentum attractors in the parameter domain ( $B$ ), as discussed later, where the dynamics is highly unstable due to the presence of a saddle of multiplicity two.

To complete the present section we now examine a new set of parameters in ( $A$ ), for which a distinct dynamical pattern connected to the saddle-center-center  $P_2$  is present, namely, the presence of oscillatory orbits that escape to the de Sitter attractor at infinity after a finite number of bounces. The parameters are

$$\begin{aligned} \Lambda &= 1, & E_r &= 0.1, \\ \alpha_{31} &= 0.002, & \alpha_{32} &= 0, & \alpha_{33} &= -0.013, \\ \alpha_{21} &= 0, & \alpha_{22} &= -13/60. \end{aligned} \quad (63)$$

For this parameter configuration the saddle-center-center  $P_2$  has coordinates  $(x_{cr_2} = 0.51007113736321, p_x = 0, y = 1, p_y = 0, z = 1, p_z = 0)$ , with the corresponding critical energy  $E_{cr_2} = 0.22015171926053$ . The initial conditions of the orbits are taken on the  $S^1$  section ( $y = 1, p_y = 0$ ) of the center manifold  $S^3$  about  $P_2$ , defined by the constraint  $\mathcal{H}_C(y = 1, p_y = 0, z, p_z, E_0) = 0$ , for the energy  $E_0 = 0.2201$ . We take, for instance,  $(z = 1.017048758412991, p_z = 0.0023417842316)$ . We evolve this initial condition forward in time, along a neighborhood of the unstable cylinder emanating from the center manifold towards the bounce as illustrated in Figures 6. The evolution of the scale factor  $x(t)$  is displayed in Fig. 6 where we see that the orbit undergoes 6 bounces before escape to the de Sitter attractor at infinity. We should note that, contrary to the set of perpetually bouncing periodic orbits examined previously, these orbits are non-periodic but oscillatory, since the values of the coordinate  $x_b$  of the bounces actually vary between  $\simeq (0.162626, 0.163973)$ , with time intervals between the 6 bounces being respec-

tively  $\Delta = [15.0, 17.7, 15.2, 16.5, 15.2]$ . The evolution of the oscillatory modes  $p_z(t)$  (left) and  $z(t)$  of the orbit of Fig. 6 is shown in Figs. 7. The frequency of the oscillatory modes increases substantially at the bounces. As the orbit approaches the de Sitter attractor the variables approach the constant values ( $z \sim 1, p_z \sim 0$ ) as expected. In fact we must remark that in our numerical evaluations the Hamiltonian constraint (46) is conserved, with a numerical error  $\leq 10^{-13}$  for the whole computational domain. In the case of the 6-bounces orbit of Figs. 6-7 the Hamiltonian constraint is violated when  $t \simeq 110.4$ , when we stop computation. At this time  $p_z = 0$  and  $z \simeq 1$ , with  $x$  sufficiently large and  $p_x \simeq 0$ .

The evolution of the anisotropy parameter for these orbits is illustrated in Figs. 8 where we plot  $\sigma^2$  for the whole time domain until the orbit reaches the de Sitter attractor. The figure at the bottom amplifies the final part of the signal showing that the shear is zero at the de Sitter attractor, as should be expected.

Finally it is worth remarking that the 6-bounces orbits of Figs. 6-7, when propagated backward in time from its initial conditions (namely, about a neighborhood of the stable cylinder) towards the bounce, would undergo just one bounce before escaping to the de Sitter attractor at infinity.

The sets of orbits discussed in the present section characterize the oscillatory and periodic modes present in the phase space dynamics of the system. We should mention that they can be related to results of Misonoh, Maeda and Kobayashi[22] modulo their use of the non-canonical variables  $(a, \beta_+, \beta_-)$ , and of a distinct parametrization, where

$$a = 2x, \quad \beta_+ = (\ln z)/6, \quad \beta_- = \sqrt{3} (\ln y)/6. \quad (64)$$

In these variables the shear parameter is expressed

$$\sigma^2 = 4 (\dot{\beta}_+^2 + \dot{\beta}_-^2).$$

We remark that, without loss of generality and for numerical simplicity, the dynamics was restricted to the invariant submanifold ( $y = 1, p_y = 0$ ).

Now we are led to examine the nonlinear extension of the stable and unstable 2-dim cylinders  $R \times S^1$ . In order to realize this construction numerically we do not make use here of the displacing (in the direction of the unstable cylinder) of initial conditions taken on the invariant center-manifold, as the shooting method in [39], but instead we make use of the instability of the motion on the center manifold which computationally conserves the Hamiltonian constraint (46) for all  $t$ , within an error  $\leq 10^{-13}$ .

In Fig. 9 we illustrate the unstable  $W_U$  (gray) and stable  $W_S$  (black) cylinders, spanned each by 26 orbits, emerging from the the center manifold section  $S^1$  towards the bounce, for a time domain corresponding to just one bounce, so that both cylinders cross just once the surface of section  $\Sigma : (x = x_b, p_x = 0)$  where  $x_b$  is the scale factor of the bounces. This numerical simulation was implemented for initial conditions ( $x_0 = x_{cr_2} =$

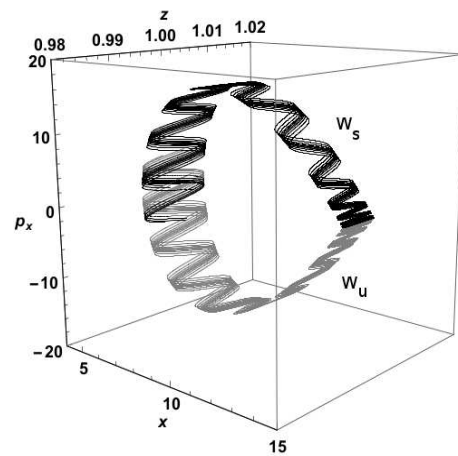


FIG. 9: A numerical illustration of the unstable cylinder (gray) and the stable cylinder (black), spanned both by 10 orbits with initial conditions taken on a circle in the domain  $(z, p_z)$  of the center manifold for  $E_0 = 9.8994$ , emerging towards the bounce. The parameter configuration is given in (61). This numerical simulation was implemented for a time domain corresponding to just one bounce, with initial conditions ( $x_0 = 14.142135621521241, p_{x_0} = 0, y_0 = 1, p_{y_0} = 0$ ), the  $(z, p_z)$  coordinates being a solution of the constraint (60).

14.142135621521241,  $p_{x_0} = 0, y_0 = 1, p_{y_0} = 0$ ) taken on  $S^1$ , with the  $(z, p_z)$  coordinates being a solution of the Hamiltonian constraint (60), for the parameters (61). Actually  $W_S$  and unstable  $W_U$  cylinders, emerging from the center manifold defined for  $E_0 = 9.8994$ , is a nonlinear extension of  $(\mathcal{T}_{E_0} \times V_S)$  and  $(\mathcal{T}_{E_0} \times V_U)$ , with  $\mathcal{T}_{E_0} \subset S^3$  defined in a linear neighborhood of  $P_2$ . These cylinders are actually composed of orbits that have the same energy  $(E_{cr_2} - E_0) \sim 10^{-5}$  of the center manifold and coalesce to it as  $t \rightarrow \pm\infty$ .

$W_S$  and  $W_U$  emanate from the center manifold towards the bounce at  $x = x_b$  and are guided by the separatrix dividing the regions  $I$  and  $II$  of the invariant plane (cf. Fig. 1). We emphasize that, in the domain (A), the separatrix  $(x(t), p_x(t))$  guiding the cylinders is actually a structure inside the cylinders about which rotational motion of the two degrees of freedom  $(y, p_y)$  and  $(z, p_z)$  take place[36, 37]. It is worth noticing that the projection of the figure in the plane  $(x, p_x)$  shadows the separatrix homoclinic to  $P_2$  in the invariant plane. These facts will be crucial in the characterization of the regular/non-chaotic dynamics of the system as discussed in the next section.

## VI. ON REGULARITY AND CHAOS IN THE INVARIANT SUBMANIFOLDS

As we have seen in the previous section the stable  $W_S$  and unstable  $W_U$  cylinders emerging from the center manifold about  $P_2$  are 4-dim surfaces so that they separate the 5-dim energy surface defined by the Hamil-

tonian constraint (46) in two dynamically disconnected pieces, a fact that is fundamental in characterization of either chaos or regular motion in the system. The occurrence of the transversal crossing of the stable cylinder and the unstable cylinder in the neighborhood of the bounce would constitute a topological characterization of chaos in the dynamics, a phenomenon that eventually leads to the formation of the Poincaré's homoclinic tangles[40].

Let us consider the first transverse intersection of the cylinders: a part of the flow inside of the unstable cylinder will enter in the interior of the stable cylinder and will be forever separated from the part of the flow that remains outside the stable cylinder. The part that remained inside the stable cylinder will proceed along the stable cylinder towards the center manifold about  $P_2$  from where it will reenter the unstable cylinder and proceeds eventually to a second bounce; by a new intersection a part of these orbits will again enter the stable cylinder and proceeds back towards the neighborhood of the center manifold, and so on. The other part of the flow outside stable cylinder will return to the neighborhood of the center manifold and there either escapes towards the de Sitter attractor at infinity or returns again towards the bounce outside the unstable cylinder. The recurrence of this process constitutes an invariant characterization of chaos in the dynamics of the system, generating horseshoe structures that appear in Poincaré maps of the system (with surface of sections  $\Sigma$  taken at the bounce  $x = x_b, p_x = 0$ ), cf. for instance [36, 37]. If we consider the transversal crossing in a section, say at the bounce ( $x = x_b, p_x = 0$ ), it is not difficult to see that the intersection is a  $S^2$ . Therefore the intersection manifold will be a 3-dim tube of flow (with the topology  $R \times S^2$ ) which is contained both in the 4-dim stable cylinder and in the 4-dim unstable cylinder, and *homoclinic* to the center-center manifold  $S^3$ . We must recall that the cylinders are actually composed of orbits that have the same energy ( $E_{cr} - E_0$ ) of the center-manifold and coalesce to it as  $t \rightarrow \pm\infty$ .

Another possibility is that the cylinders coalesce with each other: this rare situation characterizes the absence of chaos in the model and in this sense the dynamics is said to be regular/non-chaotic. Interestingly enough this is the case for the parameter domain (A) where the dynamics of the cylinders are regular as we show now. We have not found any numerical evidence of the breaking of this regular behavior, contrary for instance to the dynamics of Bianchi IX universes in bouncing braneworld cosmologies[35, 37].

To start let us consider the parameter configuration (61) used in part of the numerical experiments of the previous sections. For these parameters the saddle-center-center critical point  $P_2$  is characterized by  $E_{cr_2} = 9.89949493727457$  and ( $x_{cr_2} = 14.1421356215212$ ,  $p_x = 0$ ,  $y = 1$ ,  $p_y = 0$ ,  $z = 1$ ,  $p_z = 0$ ). The total energy of the system is taken as  $E_0 = 9.8994$  so that the energy available to the rotational degrees of freedom of the center manifold is ( $E_{cr_2} - E_0 \sim 10^{-4}$ ).

The results of the previous sections showed that two 4-dim cylinders, one stable  $W_S$  and one unstable  $W_U$ , both with the topology  $R \times S^3$ , emerge from a neighborhood of the center manifold about  $P_2$ . The center manifold  $S^3$  encloses the critical point  $P_2$  and tends to it as  $E_0 \rightarrow E_{cr_2}$ . At this limit the cylinders  $W_S$  and  $W_U$  reduce to the separatrix  $S$  which makes a homoclinic connection to itself in the invariant plane. The separatrix is a structure inside the cylinders, about which the flow with the oscillatory degrees of freedom ( $y, p_y, z, p_z$ ) proceeds guiding both cylinders towards the bounce. Their first encounter, with either a transversal crossing or a smooth coalescence is expected to occur in a neighborhood of the bounce ( $x_b = 4.565245, p_x = 0$ ) where  $x_b$  is the scale of the bounce for the orbits at  $p_x = 0$ . In order to examine this first encounter we will adopt as the surface of section[42] the 4-dim surface  $\Sigma : (x = x_b, p_x = 0)$ .

For the sake of numerical simplicity here our simulations will be restricted to the dynamics on the two 4-dim invariant submanifolds (29) and (30) of the 6-dim phase space which, in the canonical variables (43) and (44), are expressed

$$IS_1 : y = 1, p_y = 0, \quad (65)$$

$$IS_2 : y = z, p_y = 3p_z. \quad (66)$$

In the first simulation we take ( $x_0 = x_{cr_2}, p_{x0} = 0$ ), and fix the initial conditions on the 4-dim invariant submanifold  $IS_1$ , namely, with ( $y = 1, p_y = 0$ ); such initial conditions are obviously to be taken in the sector ( $z, p_z$ ) of the center manifold  $S^3$ , which has the topology of  $S^1$  and is defined by the Hamiltonian constraint (46)  $H(x = x_{cr_2}, p_x = 0, y = 1, p_y = 0, z, p_z, E_0 = 9.8994) = 0$ . By performing the evolution of 173 initial conditions in the above set, the exact dynamics actually evolves a 4-dim invariant subset ( $x, p_x, z, p_z$ ) of the full 6-dim phase space as expected due to our restriction to the 4-dim invariant submanifold ( $y = 1, p_y = 0$ ); in this particular simulation we have that, under the exact dynamics, no motion is present in the sector ( $y, p_y$ ). We generate one 2-dim stable  $W_S$  and one 2-dim unstable  $W_U$  cylinders of orbits which initially move towards the first bounce. As mentioned we adopt the surface of section  $\Sigma_b : (x = x_b, p_x = 0)$ , where  $x_b \simeq 4.565245$  is the scale factor of the bounce. The points ( $z_b, p_{z_b}$ ) resulting from the section of both cylinders ( $W_S$  black and  $W_U$  gray) by the surface of section  $\Sigma_b$  are displayed in Fig. 10 (left), corresponding actually the Poincaré maps of both cylinders on  $\Sigma_b$ . This first Poincaré map at the bounce is a numerical evidence of the coalescence of one cylinder into the other and gives a clear picture of the regular (non-chaotic) motion in the dynamics of the cylinders. We also display in Fig. 10 (right) the Poincaré maps of the cylinders in another surface of section  $\Sigma_2 = (x = 7, p_x = 15.413)$  showing also the coalescence of the two cylinders into one another in a time after the first bounce.

From these Poincaré maps we see the coalescence of the stable cylinder (black dots) and unstable cylinder (gray

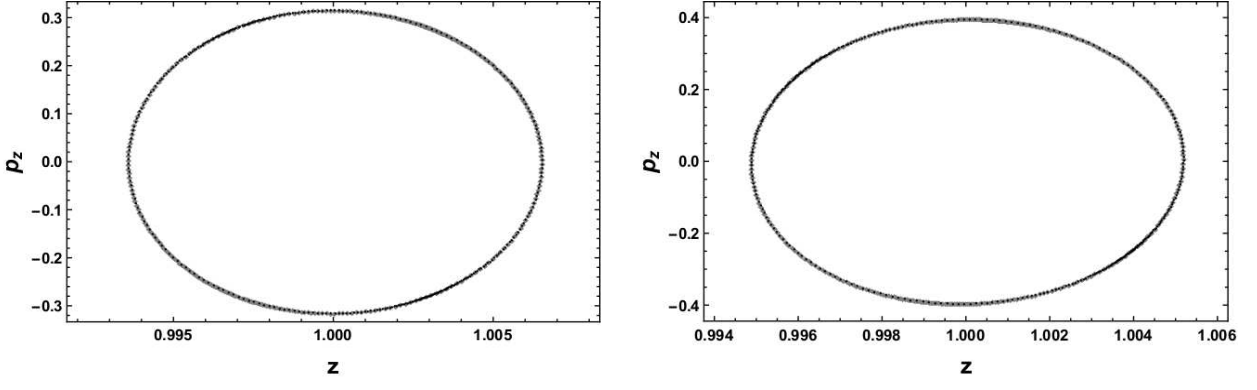


FIG. 10: (color on line) Poincaré maps of the first coalescence of the stable cylinder (black dots) and unstable cylinder (gray diamonds) in the surface of section  $\Sigma_b : (x = x_b, p_x = 0)$  at the first bounce  $x_b = 4.565245$  (left), and in the surface of section  $\Sigma_2 = (x = 7, p_x = 15.413)$  (right) shown in the plane  $(z, p_z)$ , for  $E_0 = 9.8994$ . Both cylinders were spanned by 346 orbits, with initial conditions taken on a circle in the domain  $(z, p_z)$  of the center manifold. Initial conditions and parameters are the same as in Fig. 9.

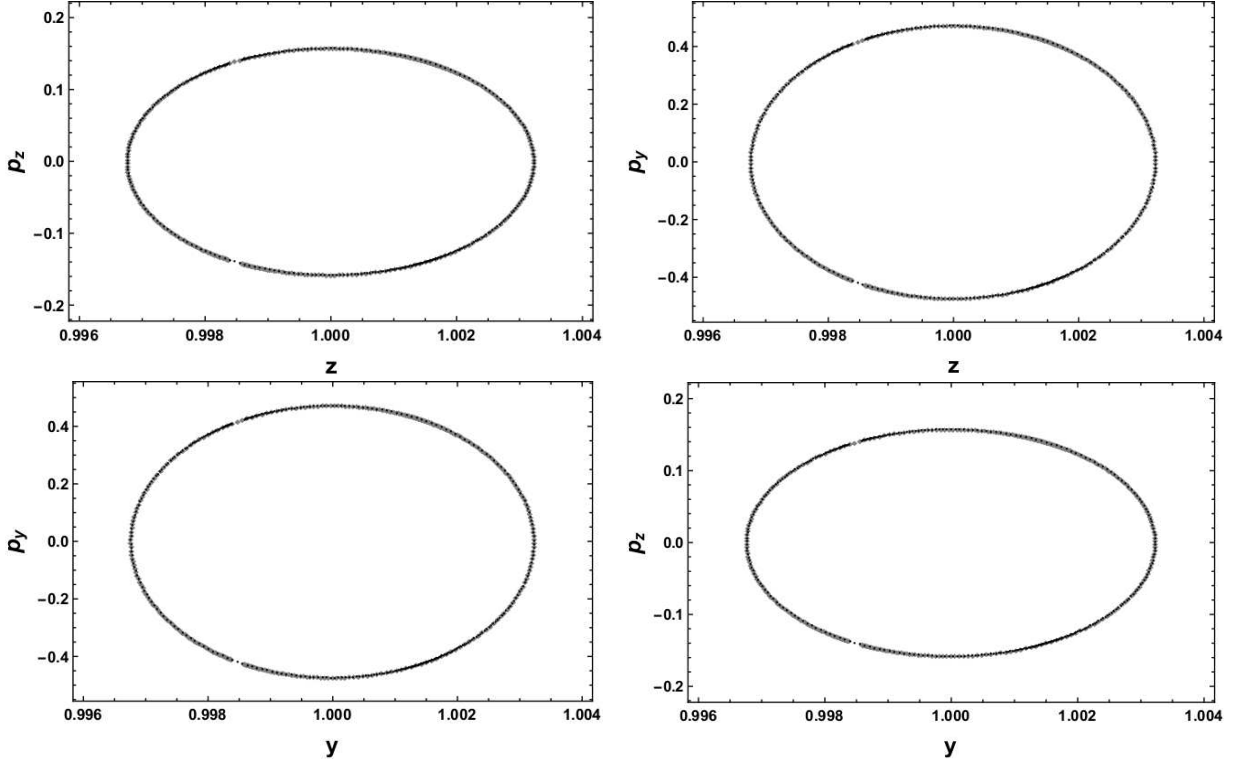


FIG. 11: (color on line) Poincaré map of the first coalescence of the stable cylinder (black dots) and unstable cylinder (gray diamonds) in the surface of section  $\Sigma_1 = (x = x_b, p_x = 0)$  (at the first bounce  $x_b = 4.56523$ ) shown in the plane  $(z, p_z)$  (1st panel),  $(z, p_y)$  (2nd panel),  $(y, p_y)$  (3rd panel) and  $(y, p_z)$  (4th panel) for  $E_0 = 9.8994$ . Both cylinders were spanned by 173 orbits, with initial conditions taken on a circle in the domain  $(z, p_z)$  of the center manifold. Here we fixed  $\Lambda = 0.001$ ,  $E_r = 10$ ,  $\alpha_{21} = -100$ ,  $A_2 = -80$ ,  $\alpha_{31} = 10^{-4}$ ,  $\alpha_{32} = 10^{-5}$ ,  $A_3 = 10^{-5}$  so that  $E_{crit} = 9.899494937274579$ .  $IS_1$  initial conditions:  $x = 14.142135621521241$ ,  $p_{x_0} = 0$ ,  $y_0 = z_0$ ,  $p_{y_0} = 3p_{z_0}$ .

diamonds) in two sections in the phase space. In fact, it can be shown that this coalescence is maintained for any section of the phase space crossed by orbits in the stable or unstable manifold. This is an integrability signature of the dynamics showing a feature of no chaos in the model. Although the numerical simulations shown here

were done for the parameters (61) we have checked that this integrability pattern is maintained in general for all parameter configurations of the domain  $(A)$  in which  $P_1$  is a center-center-center and  $P_2$  is a saddle-center-center provided by a proper choice of the coupling constants in the potential  $U_{HL}$ .

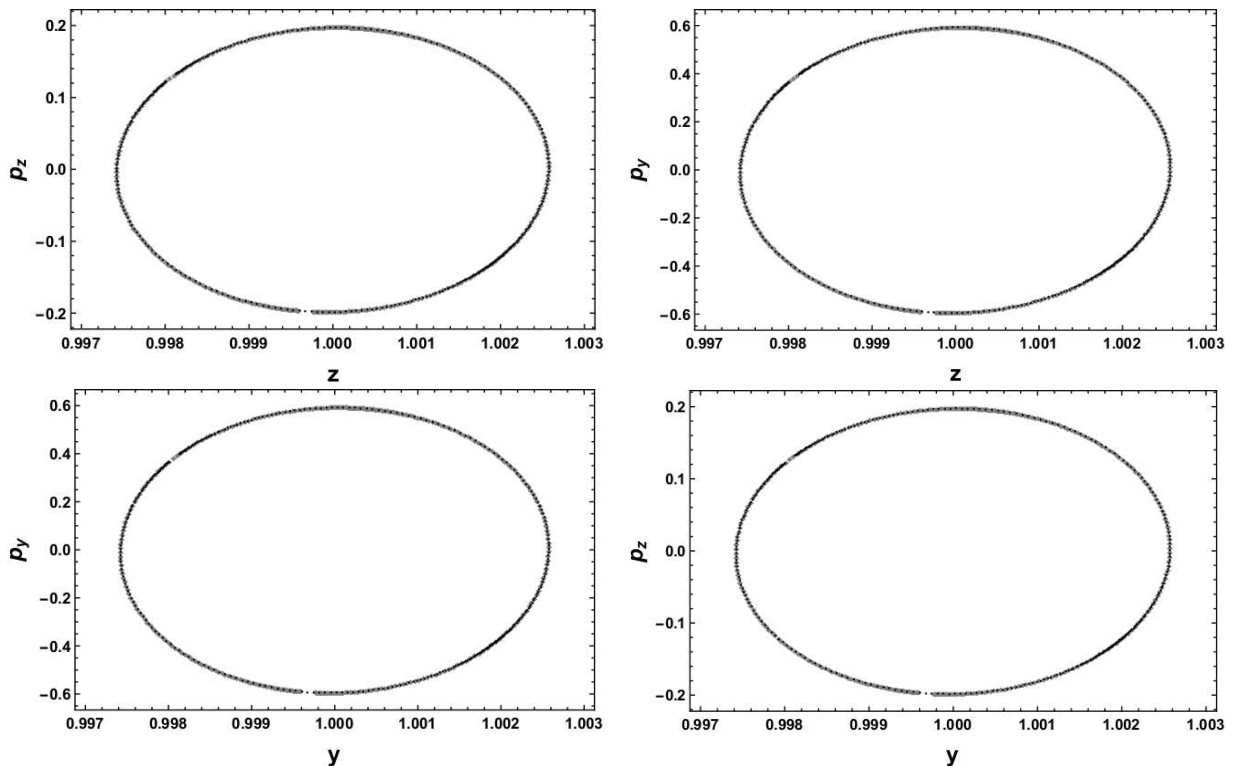


FIG. 12: (color on line) Poincaré map of the first coalescence of the stable cylinder (black dots) and unstable cylinder (gray diamonds) in the surface of section  $\Sigma_2 = (x = 7, p_x = 15.4131)$  shown in the plane  $(z, p_z)$  (1st panel),  $(z, p_y)$  (2nd panel),  $(y, p_y)$  (3rd panel) and  $(y, p_z)$  (4th panel) for  $E_0 = 9.8994$ . Both cylinders were spanned by 173 orbits, with initial conditions taken on a circle in the domain  $(z, p_z)$  of the center manifold. Here we fixed  $\Lambda = 0.001$ ,  $E_r = 10$ ,  $\alpha_{21} = -100$ ,  $A_2 = -80$ ,  $\alpha_{31} = 10^{-4}$ ,  $\alpha_{32} = 10^{-5}$ ,  $A_3 = 10^{-5}$  so that  $E_{cr} = 9.899494937274579$ .  $IS_1$  initial conditions:  $x = 14.142135621521241$ ,  $p_{x_0} = 0$ ,  $y_0 = z_0$ ,  $p_{y_0} = 3p_{z_0}$ .

To complete our analysis we have also considered the case of the second invariant submanifold  $IS_2$ . Again we obtain here numerical evidence of the regularity of the dynamics as given in Figs. 11 and 12. Here we plot the Poincaré maps in the surface of section  $\Sigma_b : (x = x_b, p_x = 0)$  at the first bounce (corresponding to the points  $(y_b, p_{y_b}, z_b, p_{z_b})$ ) of the stable cylinder (black dots) and the unstable cylinder (gray diamonds) as shown in Figure 5, and in the surface of section  $\Sigma_2 = (x = 7, p_x = 15.4131)$ . corresponding to the points  $(y_b, p_{y_b}, z_b, p_{z_b})$  as shown in Fig. 6. These Poincaré maps show clearly the coalescence of the stable cylinder (black dots) and unstable cylinder (gray diamonds) in two arbitrary sections in the phase space, in common with the case of the first invariant submanifold  $IS_2$ . As in the previous experiments we verified numerically that this coalescence is maintained for any surface of section of the phase space crossed transversally by the stable and the unstable manifolds. This is a regular signature of the dynamics showing a feature of no chaos in the model. Furthermore we also checked that this regular (non-chaotic) pattern of the dynamics, obtained for the invariant submanifold  $IS_2$  with the parameters (61), is maintained in general for parameter configurations (A) in which  $P_1$  is a center-center-center and  $P_2$  is a saddle-center-center.

The patterns of the phase space dynamics of a general Bianchi IX cosmological model discussed in the previous sections are fundamentally connected to the general potential  $U_{HL}$  (5) of a non-projectable version of Horava-Lifshitz gravity which, among other characteristics, allows for the presence of nonsingular bounces in the orbits of the model due to curvature dependent potentials.

The rich dynamics of the model is mainly due to the number of parameters introduced via the HL potential which in turn demands a careful classification of the pairs of critical points in the finite region of the phase space. In the domain of parameters (A) examined in sections IV, V and VI the critical points are a center-center-center and a saddle-center-center so that the phenomena in phase space are of the same nature of the ones discussed in [22, 36, 37]. Now in the following two sections we will examine the parameter domains (B) and (C) in which some features of the phase space dynamics – mainly connected to the presence of a saddle with multiplicity two – are new and, to our knowledge, not yet seen in the literature.

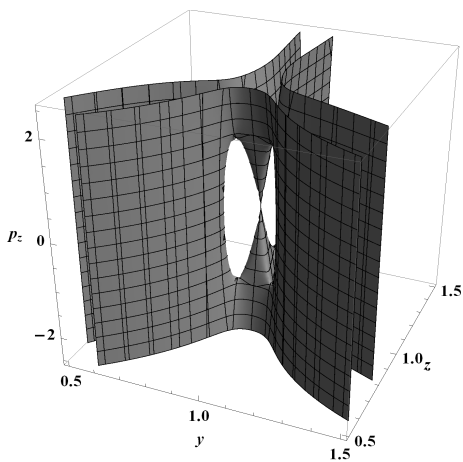


FIG. 13: Numerical illustration of the phase space in a neighborhood of the center-saddle-saddle  $P_1$ , corresponding to the parameter configuration (67). Here we display the section ( $x = x_{cr1} = 7.071067829543$ ,  $p_x = 0$ ,  $p_y = 0$ ) of the 5-dim phase space for  $E_0 = E_{cr1}$ . The critical point  $P_1$  is located at the common vertex of the cones into which the 4-hyperboloid degenerates for  $E_0 = E_{cr}$ . The high instability of the dynamics outside the invariant plane is due to the presence of a saddle of multiplicity two at  $P_1$ .

## VII. A SADDLE OF MULTIPLICITY TWO AND THE $P_Z$ -MOMENTUM ATTRACTORS

Here our focus will be in the parameter domain ( $B$ ) where  $P_1$  is a center-saddle-saddle and  $P_2$  is a saddle-center-center. The topology of the phase space in the neighborhood of  $P_1$  has the structure of a saddle of multiplicity two times  $S^1$ , since  $P_1$  in ( $B$ ) has  $q < 0$  and  $q_x < 0$  (cf. (48)). This topological feature induces a high instability in the phase space dynamics. In order to better grasp such behavior we illustrate in Fig. 13 the topology of the phase space about  $P_1$  with the parameters

$$\begin{aligned} \Lambda &= 0.001, & E_r &= 1, \\ \alpha_{31} &= 10^{-4}, & \alpha_{32} &= 10^{-5}, & \alpha_{33} &= -0.00092, & (67) \\ \alpha_{21} &= 0, & \alpha_{22} &= -248/3, \end{aligned}$$

with  $x_{cr1} = 7.071067829543$  and  $E_{cr1} = 9.192388160728$ . While on the invariant plane the motion about  $P_1$  is that of periodic orbits, outside the invariant plane the hyperbolic motion is the origin of a high instability in the phase space dynamics. Fig. 13 displays the phase space section ( $x = x_{cr1}$ ,  $p_x = 0$ ,  $p_y = 0$ ) of the hyperbolic motion about  $P_1$ . In the figure we note that the critical point  $P_1$  is located at the common vertex of cones into which the 4-hyperboloid degenerates for  $E_0 = E_{cr1}$ .

Let us now discuss some new features in the dynamics of orbits visiting a nonlinear neighborhood of  $P_1$  connected with its character of a saddle of multiplicity two.

For the parameters (67) adopted, let us consider the saddle-center-center critical point  $P_2$  : ( $x = x_{cr2} =$

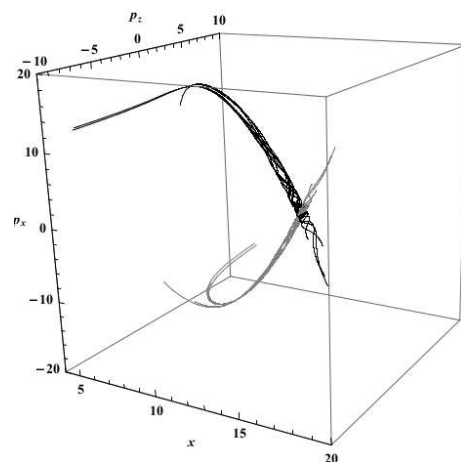


FIG. 14: Numerical illustration of the unstable cylinder (gray) and stable cylinder (black), that emerge from a neighborhood of  $P_2$  towards the bounce, spanned each by 26 orbits with initial conditions taken on a circle in the domain ( $z, p_z$ ) of the center manifold about  $P_2$  for  $E_0 = 9.8994$ , corresponding to the parameters (67). The projection of the figure in the plane ( $x, p_x$ ) “shadows” the separatrix of the invariant plane. Due to the instability in the dynamics connected to the saddle with multiplicity two in  $P_1$ , part of the orbits escape to two additional  $p_z$ -momentum attractors with an infinitely large anisotropy parameter, at  $x = \text{const}$ ,  $z = \text{const}$  and  $p_z \rightarrow \pm\infty$ , as shown in the figure.

14.14213562152124,  $p_x = 0$ ,  $y = 1$ ,  $p_y = 0$ ,  $z = 1$ ,  $p_z = 0$ ) with critical energy  $E_{cr2} = 9.89949493727457$ . We construct the unstable cylinder  $W_U$  (gray) that emerges from the neighborhood of  $P_2$  towards the bounce, spanned by 26 orbits, with initial conditions taken on a circle in the domain ( $z, p_z$ ) of the center manifold about  $P_2$  with energy  $E_0 = 9.8994$ . From the same initial conditions we generate the stable cylinder  $W_S$  (black) that also emerges towards the bounce. These cylinders are illustrated in Fig. 14 from where three distinct sets of orbits can be singled out. According to the dynamics examined in previous sections, these orbits would be expected to have two attractors, either the center manifold itself or the de Sitter attractors at infinity. These two set of orbits (connected with the deSitter or the center manifold attractors) are seen in the Figure, the projection of which on the invariant plane ( $x, p_x$ ) “shadows” the separatrix of the invariant plane.

However in the present case ( $B$ ), due to the high instability connected to the saddle-saddle-saddle  $P_1$ , we observe a third set of orbits that visit a nonlinear neighborhood of  $P_1$  and escape to two additional  $p_z$ -momentum attractors with a very large anisotropy parameter at  $x = \text{const.}$ ,  $z = \text{const.}$  and  $p_z \rightarrow \pm\infty$  as can also be seen in Fig. 14. Due to the high instability of the dynamics of these orbits, the numerical evaluation for long times is quite critical, demanding an accuracy which is in the available limit of the codes used in this work. Let us consider, for instance, an orbit on the unstable cylin-

der belonging to this third set, generated from the initial conditions

$$\begin{aligned} x &= x_{cr2}, \quad p_x = 0, \quad y = 1, \quad p_y = 0, \\ z &= 1.00075, \quad p_z = 0.5954540145554457, \end{aligned} \quad (68)$$

taken on the circle  $(z, p_z)$  of the section  $(y = 1, p_y = 0)$  of the center manifold about  $P_2$ , for  $E_0 = 9.8994$ . We kept the dynamics restricted to the time interval  $t = [0, 477.39]$  so that the Hamiltonian constraint  $\mathcal{H}$  (46) is still conserved, namely,  $\mathcal{H} \leq 3.337 \times 10^{-12}$ . At  $t = 477.39$  we obtain  $x \simeq 4.51755$ ,  $z \simeq 0.201023$  and  $p_z \simeq 910.195$ , leading to a value of the anisotropy parameter  $\sigma^2 \simeq 3.93864$  which is larger than the initial anisotropy by eight orders of magnitude. For  $t$  slightly larger than  $t_f = 477.39$  the conservation of  $\mathcal{H}$  breaks up, with the value of  $p_z$  increasing exponentially. We therefore conclude that the asymptotic configuration of the orbits of the third set, shown in Fig. 14, escape to two  $p_z$ -momentum attractors with an infinitely large anisotropy parameter, at  $x = \text{const}$ ,  $z = \text{const}$  and  $p_z \rightarrow \pm\infty$ . This is a direct consequence of the dynamical instability associated with the saddle of multiplicity two at  $P_1$ , a feature not yet observed in the results of the previous Sections.

Finally we must note that in our present example the dynamics of the orbits is restricted to the invariant submanifold  $(y = 1, p_y = 0)$ , so that the anisotropy parameter reduces to  $\sigma^2 = (z^2 p_z^2 / x^6)$ , cf. (62).

### VIII. THE CENTER MANIFOLD ABOUT A SADDLE OF MULTIPLICITY TWO: PARAMETRIC BIFURCATION

Finally we discuss here the phase space dynamics corresponding to a system whose parameter configuration is in the domain  $(C)$ . As we will see the skeleton of the dynamics is dominated by the saddle-saddle-saddle critical point  $P_2$ , and the effect of the saddle with multiplicity two on the dynamics about  $P_2$  is examined. We should mention that the presence of a saddle of multiplicity two in physical systems is rare (possibly absent in the case of cosmological models) and therefore we are led to undertake a more detailed examination of this case. Let us consider the following parametric configuration in  $(C)$

$$\begin{aligned} \Lambda &= 5/60, \quad Er = 0, \\ \alpha_{31} &= 0.1, \quad \alpha_{32} = 0, \quad \alpha_{33} = 1, \\ \alpha_{21} &= 1.4601, \quad \alpha_{22} = 1/3, \end{aligned} \quad (69)$$

for which we obtain the two critical points  $P_1$  and  $P_2$  with

$$\begin{aligned} x_{cr1} &= 0.715744514081549, \\ x_{cr2} &= 2.09499845891933, \end{aligned}$$

corresponding to the two positive real roots of equation (27). For  $P_1$  we obtain that the energy  $E_{cr1} < 0$  so

that this critical point is out of the physical phase space. Therefore in the parameter configuration (69) the physical system has only one critical point  $P_2$ , the energy of which is

$$E_{cr2} = 0.00001411994285. \quad (70)$$

For  $P_2$  we also evaluate that

$$q = -0.00267275969793, \quad q_x = 1.32604264858754, \quad (71)$$

characterizing  $P_2$  as a saddle-saddle-saddle (where a saddle with multiplicity two is present, cf. (47)). The critical point  $P_2$ , which is denoted a saddle-saddle-saddle, corresponds actually to the topological product of a saddle times a saddle with multiplicity two. Therefore, to avoid a saturation in the remaining text, we will sometimes refer to  $P_2$  simply as a saddle with multiplicity two. We now proceed to examine the topology of the phase space about this critical point.

To start let us examine the possible linear motions about  $P_2$ . Let us consider the case  $E_x = 0$ , cf. (51). The first possibility corresponds to  $(x = x_{cr2}, p_x = 0)$  implying that the motions are orbits on the 3-dim surfaces

$$\begin{aligned} \left[ \frac{1}{2} \frac{p_y^2}{M_0^3} - 3|q|(y-1)^2 \right] + \left[ \frac{3}{2} \frac{p_z^2}{M_0^3} - |q|(z-1)^2 \right] \\ = 2(E_{cr2} - E_0), \end{aligned} \quad (72)$$

which depend continuously on  $E_0$ . For  $(E_{cr2} - E_0)$  sufficiently small so that (72) holds, these constant energy surfaces have the structure of a 3-hyperboloid with the constant of motions  $C_1$ ,  $C_2$  and  $C_3$  satisfying the algebra of the three-dimensional hyperboloid group under the Poisson bracket operation (cf. (58) with  $q < 0$ ). However, contrary to the cases of the previous sections where the  $S^3$  center manifold reduces to the critical point as  $E_0 \rightarrow E_{cr2}$ , here the 3-hyperboloid invariant manifold consists of the critical point from which emanate the saddle lines  $p_y = \pm\sqrt{3}\mu(y-1)$  and  $p_z = \pm(\mu/\sqrt{3})(z-1)$  with multiplicity two, where  $\mu = \sqrt{2|q|M_{0z}^3}$ . Actually in the case of  $E_0 = E_{cr2}$  the hyperbolic phase space dynamics about a neighborhood of the critical point is analogous to that illustrated in Fig. 13, where there 3-hyperboloid degenerates into two 3-cones with a common vertex at the critical point. The nonlinear extension of the center manifold, obtained as  $(E_{cr2} - E_0)$  increases, exhibits a rich structure connected to the presence of a saddle with multiplicity two and its bifurcations, as we now proceed to discuss.

For the configurations analyzed in the previous sections, for which  $P_2$  had  $q > 0$ , the existence of the center manifold demanded that  $E_{cr2} - E_0 \geq 0$ ; for the equality case the center manifold reduced to a point, the saddle-center-center critical point. Now since  $q < 0$  this restriction no longer exists as can be clearly seen from (72). Our analysis will contemplate separately the following energy

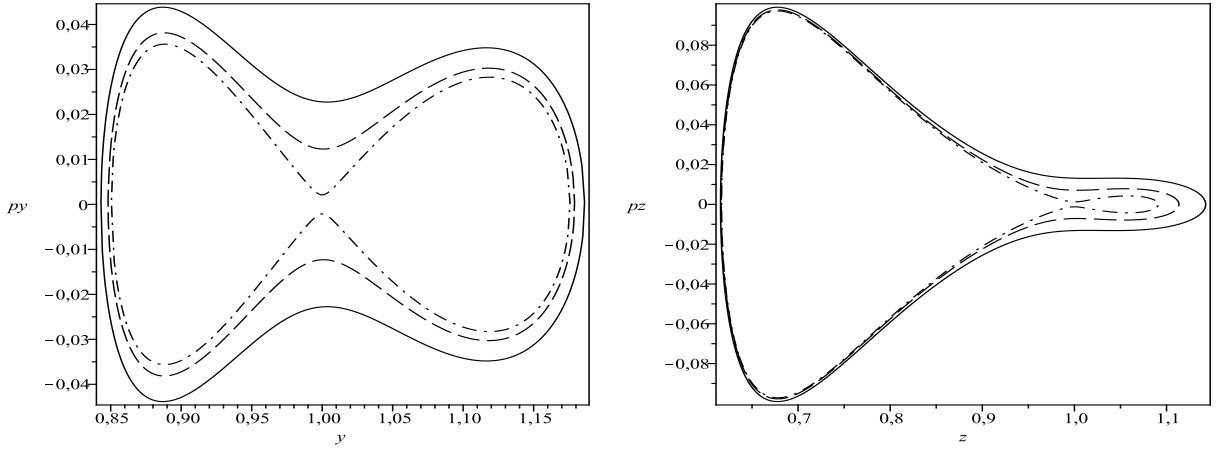


FIG. 15: Section ( $p_z = 0, z = 1$ ) (left) and section ( $p_y = 0, y = 1$ ) (right) of the 3-dim center manifold (74) for  $E_0 = 0$  (solid), 0.00001 (dashed) and 0.000014 (dash-dotted), corresponding to the parameter configuration (69) with  $q < 0$ . For these energies  $E_0 < E_{cr_2}$  the manifold is topologically a 3-sphere enclosing the critical point  $P_2$  which is a saddle-saddle-saddle. As  $E_0 \rightarrow E_{cr_2}$  the curves pinch at the critical point  $P_2$ , corresponding to ( $y = 1, p_y = 0$ ) (left figure) and ( $z = 1, p_z = 0$ ) (right figure).

domains,

$$\begin{aligned}
 (I) : & \quad (E_{cr_2} - E_0) > 0, \\
 (II) : & \quad E_{cr_2} - E_0 = 0, \\
 (III) : & \quad E_{cr_2} - E_0 < 0.
 \end{aligned} \tag{73}$$

In the energy domains (73) the 3-dim center manifold about  $P_2$  (containing a saddle of multiplicity two) is given by the Hamiltonian constraint,

$$\begin{aligned}
 \mathcal{H}_C = & \frac{p_y^2 y^2}{2x_{cr_2}^3} + \frac{3p_z^2 z^2}{2x_{cr_2}^3} + \frac{x_{cr_2}}{2z^{\frac{4}{3}}} - \frac{x_{cr_2}}{yz^{\frac{1}{3}}} - \frac{x_{cr_2} y}{z^{\frac{1}{3}}} \\
 & - x_{cr_2} z^{\frac{2}{3}} + \frac{x_{cr_2} z^{\frac{2}{3}}}{2y^2} + \frac{1}{2} x_{cr_2} y^2 z^{\frac{2}{3}} + 2x_{cr_2}^3 \Lambda \\
 & + 2E_0 + \frac{2E_r}{x_{cr_2}} + x_{cr_2}^3 U_{HL}(x_{cr_2}, y, z) = 0.
 \end{aligned} \tag{74}$$

In the energy domain (I) the 3-dim surface (74) is a topological 3-sphere enclosing the saddle with multiplicity two  $P_2$ , as illustrated in Figs. 15, where we plot its sections ( $p_z = 0, z = 1$ ) (left) and section ( $p_y = 0, y = 1$ ) (right), for  $E_0 = 0$  (solid), 0.00001 (dashed) and 0.000014 (dash-dotted). As  $E_0 = E_{cr_2}$  the curves pinch at the critical point  $P_2$ , corresponding to ( $y = 1, p_y = 0$ ) (left figure) and ( $z = 1, p_z = 0$ ) (right figure). A larger dimensional view of this case is also illustrated in Fig. 16, (top, left), where we plot the 2-dim section  $p_y = 0$  of the invariant 3-dim center manifold (74) for  $E_0 = 0$ , showing a topological  $S^3$  (with three lobes) enclosing the saddle with multiplicity two.

As  $E_0$  increases towards the value  $E_{cr_2}$  the closed surface deforms, reaching the domain (II) : ( $E_0 = E_{cr_2}$ ) when the closed surface *pinches* at the critical point  $M_0 = (x = x_{cr_2}, p_x = 0, y = 1, p_y = 0, z = 1, p_z = 0)$ ,

as shown in Fig. 16, (top, right). In this case the center manifold is said to undergo a bifurcation; the saddle with multiplicity two  $P_2$  now belongs to (74), being a common point of the lobes and breaking the  $S^3$  topology, so that this manifold contains infinitely many homoclinic orbits to the critical point.

As the energy parameter enters the domain III :  $E_0 > E_{cr_2}$  a further bifurcation occurs and the 3-dim manifold becomes topologically a 3-torus, as illustrated in Fig. 16 (bottom, left), showing the bifurcation of a  $S^3$  into a 3-torus. The critical point is outside the 3-torus. Finally, for larger values of  $E_0$  in the domain (III) the invariant center manifold becomes multiply connected, Fig. 16, (bottom, right).

The above picture is in bold contrast with the case of a center-center with multiplicity two, examined in Sections IV-V, where the 3-dim center manifold about this critical point is defined for  $0 \leq E_0 \leq E_{cr_2}$  and reduces to a single point (the critical point) for  $E_0 = E_{cr_2}$ . For  $E_0 > E_{cr_2}$  the center manifold does not exist.

A more extended examination of these structures and the associated features of the whole phase space dynamics, as well as its implications to Cosmology, is beyond the scope of the present paper and will be dealt with in a future work. However we should mention that, to our knowledge, such features have not yet been seen in the literature of cosmological models.

## IX. FINAL COMMENTS AND CONCLUSIONS

In this paper we examined the phase space dynamics of general bouncing Bianchi IX cosmological models in which nonsingular bounces are generated by extra higher order spatial curvature terms in the framework of the Hořava-Lifshitz (HL) gravity. The HL grav-

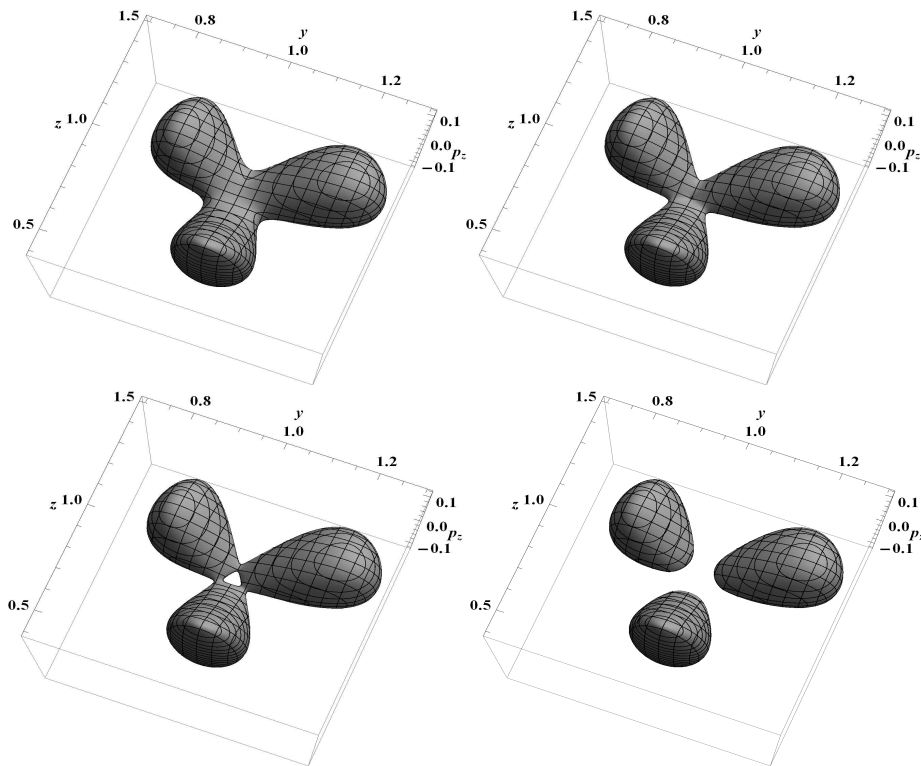


FIG. 16: The 2-dim sections  $p_y = 0$  of the 3-dim center manifold (74) for several significant energies: (i)  $E_0 = 0$  (top, left): (74) has the topology of a  $S^3$  enclosing the saddle with multiplicity two, a pattern which holds for the domain  $0 \leq E_0 < E_{cr2}$ . (ii)  $E_0 = E_{cr2}$  (top, right): the saddle with multiplicity two now belongs to (74), being the one point connection of two leaves of the manifold and breaking the  $S^3$  topology, so that this manifold contains infinitely many homoclinic orbits. (iii)  $E_0 = 0.0000153 > E_{cr2}$  (bottom, left): showing the bifurcation of  $S^3$  into a 3-dim torus. The critical point is outside the 3-torus. (iv) for larger values,  $E_0 = 0.000025$  (bottom, right): the center manifold becomes multiply connected. The parameters of this configuration are given in (69).

ity action adopted contains five independent parameters, apart from the  $\lambda$  parameter that breaks the invariance under four-dimensional diffeomorphisms present in classical General Relativity. In order to recover the classical regime, our analysis was restricted to  $\lambda = 1$ . In the  $U_{HL}({}^3R)$  potential considered in the paper the five independent parameters were restricted by imposing  $A_3 > 0$  (cf. (25)) so that the dynamics is nonsingular implementing instead bounces in the dynamics of the model. Furthermore in the class of models analyzed we have restricted ourselves to an energy-momentum tensor of dust and radiation, which are conserved independently, plus a positive cosmological constant  $\Lambda$ . The corresponding total energy of dust turns out to be a constant of motion connected to the total conserved Hamiltonian. As a consequence of  $A_3 > 0$  and  $\Lambda > 0$  the model contains just two critical points  $P_1$  and  $P_2$  at the finite region of the phase space. The nature of these critical points determines the structure of the phase space dynamics and of the attractors at infinity.

Our treatment in the paper is based strongly on the Hamiltonian formulation, with a conserved Hamiltonian constraint plus the associated Hamilton's equations of motion. By the use of appropriate canonical variables we

were able to make a global examination of the structures of the phase space that organize the dynamics, as critical points, center manifolds, homoclinic cylinders emanating from the center manifolds and the attractors at phase space infinity.

In Section III the nature of the critical points in the 6-dim phase space was examined by the linearization of Hamilton equations about these points. In this context we were able to classify the dynamics in four distinct parameter domains according to the possible nature of the critical points: domain (A), where the critical point  $P_1$  is a center-center-center and the critical point  $P_2$  is a saddle-center-center; domain (B), where  $P_1$  is a center-saddle-saddle and  $P_2$  is a saddle-center-center; domain (C), where  $P_1$  is a center-saddle-saddle and  $P_2$  is a saddle-saddle-saddle; domain (D), where  $P_1$  is a center-center-center and  $P_2$  is a saddle-saddle-saddle. In all four domains, with its respective structures of critical points and of attractors at infinity, the Bianchi IX models are non-singular in the sense that the spacetime curvature does not diverge and the physical average scale factor  $x(t)$  never reaches zero. All phase space orbits discussed in the paper are either periodic (perpetually bouncing solutions), or oscillatory with an eventual escape to one

of the attractors at the infinity of phase space, or orbits homoclinic to a center manifold.

The features of the parameter domain ( $A$ ) were examined in Sections IV-VI. The critical points are a center-center-center  $P_1$  and a saddle-center-center  $P_2$ . We introduced a new set of canonical variables  $(x, p_x, y, p_y, z, p_z)$  that separate the degrees of freedom of the system into two rotational modes  $(y, p_y)$  and  $(z, p_z)$ , about a linear neighborhood of the center-center sector of both critical points and an expansion/contraction mode  $(x, p_x)$  along the saddle direction of  $P_2$  or a further rotational mode along the additional center direction of  $P_1$ . The rotational modes for both critical points, connected to the presence of a center of multiplicity two, are defined on the *center manifold* of unstable periodic orbits which has the topology  $S^3$ . A necessary condition for the existence of the center manifold is  $(E_{cr} - E_0) > 0$ , where  $E_{cr}$  is the energy of the critical point and  $E_0$  is the total energy of the system. By continuity as  $(E_0 - E_{cr})$  increases the nonlinear extension of the center manifold maintains the topology of  $S^3$ . In the case of  $P_2$ , together with the saddle variables  $(x, p_x)$  it defines the 4-dim stable and unstable cylinders, with topology  $R \times S^3$  that coalesce to the center manifold as  $t \rightarrow \pm\infty$  respectively. Summing up, the topology of the phase space about the center-center-center  $P_1$  is  $S^1 \times S^3$  and about the saddle-center-center  $P_2$  is  $R \times S^3$ . Therefore in a neighborhood of  $P_2$  the variables  $(x, p_x)$  have a saddle nature, while in the neighborhood of  $P_1$  they have a rotational nature. With the use of the canonical variables  $(y, p_y, z, p_z)$  we obtain an exact analytical form for the center manifold as well as an accurate numerical description of the phase space dynamics in extended regions away from the critical points.

In Section V we then considered two characteristic types of orbits obtained from distinct sets of parameters in the domain ( $A$ ) and appropriate initial conditions on the center manifold. The first case corresponds to perpetually bouncing periodic orbits (propagated forward or backward in time) and the second case corresponds to oscillatory orbits that undergo a finite number of bounces before escaping to the deSitter attractor at infinity. In both cases the frequency of the oscillatory modes of the orbit increases substantially as it visits the neighborhood of the bounces. We also examined the evolution of the anisotropy parameter which is connected with the rotational mode variables. We obtained that the anisotropy is oscillatory and bounded, increasing several orders of magnitude as the orbits visit a neighborhood of the bounce. In particular the anisotropy of the second set of orbits, with a finite number of bounces, goes to zero as the orbits reach the deSitter attractor. This parameter will be useful in the recognition of the nature of anisotropic momentum attractors that appear in the domain parameter ( $B$ ). Also, for the parameter domain ( $A$ ), we examined in Section VI the question of regular and/or chaotic motion connected to the 4-dim homoclinic cylinder structures emanating from the center manifold

about  $P_2$ . Contrary to results of homoclinic chaos originated from the transversal crossings of homoclinic cylinders in Bianchi IX bouncing brane cosmologies[35, 37], in the present set of Hořawa-Lifshitz Bianchi IX bouncing cosmologies we obtained the smooth coalescing of the stable and the unstable homoclinic cylinders, characterizing thus a regular dynamics in the invariant submanifolds of the model. This is a rare result of the regularity of the dynamics in the presence of homoclinic cylinders, not yet seen in the literature of cosmological models.

Completely new distinct dynamical patterns appear in connection with the critical points in the parameter domains ( $B$ ) and ( $C$ ). In the case of ( $B$ ) the two critical points are a center-saddle-saddle  $P_1$  and a saddle-center-center  $P_2$ . As discussed in detail in Sections IV-V, in a neighborhood of a saddle-center-center  $P_2$  we have the general pattern of stable and unstable cylinders of orbits emanating from the center manifold about  $P_2$ . However in the present case the critical point  $P_1$  contains a saddle of multiplicity two which is the source of a high instability in the dynamics, acting on the cylinders as they visit a nonlinear neighborhood of  $P_1$ . In fact our numerical experiments showed that orbits of stable and unstable cylinders emerging from the center manifold about  $P_2$  towards the bounce can be classified in three distinct sets according to their attractors: (i) orbits that have the center manifold as an attractor, (ii) orbits that have the de Sitter configurations at infinity as an attractor and (iii) the two further attractors at  $p_z \rightarrow \pm\infty$ . The momentum attractors (iii) correspond to a configuration of infinite anisotropy; this is a direct consequence of the dynamical instability associated with the saddle of multiplicity two at  $P_1$ , a feature not observed in the results of the previous Sections.

In Section VIII we discussed the properties of the center manifold about the saddle-saddle-saddle critical point  $P_2$ , in the case of the parameter configuration ( $C$ ). The presence of a saddle of multiplicity two in  $P_2$  engenders a rich structure in the phase space not yet observed in the literature. Contrary the previous cases – where the 3-dim center manifold is defined for  $0 \leq E_0 \leq E_{cr_2}$  only and reduces to a single point (the critical point) for  $E_0 = E_{cr_2}$  – the center manifold is defined for all  $E_0 \geq 0$  and undergoes bifurcations with increasing  $E_0$ . For  $E_0 < E_{cr_2}$  the topology of the center manifold is  $S^3$  enclosing the critical point  $P_2$ . For  $E_0 = E_{cr_2}$  it turns into a  $S^3$  with two points identified with  $P_2$ . In this case the center manifold contains infinitely many orbits homoclinic to the critical point  $P_2$ . For  $E_0 > E_{cr_2}$  the manifold turns into a topological torus. Finally for  $E_0$  sufficiently large the center manifold becomes multiply connected with three distinct lobes. The dynamics in the whole phase is highly unstable and its detailed examination is beyond the scope of the present paper. It will eventually be discussed in a future publication.

Finally the fourth parameter domain ( $D$ ) was not examined since most of its features are present already in the other domains.

## Acknowledgements

The authors acknowledge the partial financial support of CNPq/MCTI-Brazil. The Figures were generated us-

ing the Wolfram Mathematica 7 and the Dynamics Solver packet [43].

- 
- [1] V. Mukhanov, *Physical Foundations of Cosmology* (Cambridge University Press, 2005).
- [2] S. Weinberg, *Cosmology* (Oxford University Press, 2008).
- [3] D. Gorbunov and V. Rubakov, *Introduction to the Theory of the Early Universe: Hot Big Bang Theory* (World Scientific Publishing Company, 2011).
- [4] P. Peter and J-P Uzan, *Primordial Cosmology* (Oxford University Press, 2013).
- [5] R. M. Wald, *General Relativity* (University of Chicago Press, Chicago, 1984).
- [6] R. Penrose, Phys. Rev. Lett. **14**, 57 (1965).
- [7] L. F. Abbott and So-Young Pi, *Inflationary Cosmology* (World Scientific Publishing, 1986).
- [8] A. G. Riess et al., Astron. J. **116**, 1009 (1998); S. Perlmutter et al., Astrophys. J. **517**, 565 (1999); J.L. Tonry et al., Astrophys. J. **594**, 1 (2003); M.V. John, Astrophys. J. **614**, 1 (2004); P. Astier et al., Astron. Astrophys. **447**, 31 (2006); A.G. Riess et al., Astrophys. J. **659**, 98 (2007); D. Rubin et al., Astrophys. J. **695**, 391 (2009); M. Hicken et al., Astrophys. J. **700**, 1097 (2009).
- [9] S. Weinberg, Rev. Mod. Phys. **61**, 1 (1989).
- [10] M. Novello and S. E. Perez Bergliaffa, Phys. Rep. **463**, 127 (2008).
- [11] D. Battefeld and P. Peter, Phys. Rep. **571**, 1 (2015).
- [12] R. Brandenberger and P. Peter, Found. Phys. **47**, 797 (2017).
- [13] R. C. Tolman, Phys. Rev. **38**, 1758 (1931); G. Murphy, Phys. Rev. D **8**, 4231 (1973); M. Novello and J. M. Salim, Phys. Rev. D **20**, 377 (1979); V. Melnikov and S. Orlov, Phys. Lett. A **70**, 263 (1979); J. Acacio de Barros, N. Pinto-Neto, and M. A. Sagiuro-Leal, Phys. Lett. A **241**, 229 (1998); R. Colistete Jr., J. C. Fabris, and N. Pinto-Neto, Phys. Rev. D **62**, 083507 (2000); J. Khoury, B.A. Ovrut, P. J. Steinhardt, and N. Turok, Phys. Rev. D **64**, 123522 (2001); V.A. De Lorenci, R. Klippert, M. Novello, and J. M. Salim, Phys. Rev. D **65**, 063501 (2002); F.G. Alvarenga, J. C. Fabris, N. A. Lemos, and G. A. Monerat, Gen. Relativ. Gravit. **34**, 651 (2002); J. C. Fabris, R. G. Furtado, P. Peter, and N. Pinto-Neto, Phys. Rev. D **67**, 124003 (2003); A. Ashtekar, M. Bojowald, and J. Lewandowski, Adv. Theor. Math. Phys. **7**, 233 (2003); T. Biswas, R. Brandenberger, A. Mazumdar, and W. Siegel, J. Cosmol. Astropart. Phys. **12** (2007) 011; L.R. Abramo, P. Peter, and I. Yasuda, Phys. Rev. D **81**, 023511 (2010); P. Peter and N. Pinto-Neto, Phys. Rev. D **78**, 063506 (2008); Yi-Fu Cai, R. Brandenberger, and X. Zhang, J. Cosmol. Astropart. Phys. **03** (2011) 003.
- [14] Rodrigo Maier, Stella Pereira, Nelson Pinto-Neto, and Beatriz B. Siffert, Phys. Rev. D **85**, 023508 (2012).
- [15] Rodrigo Maier, Nelson Pinto-Neto and Ivano Damião Soares, Phys. Rev. D **87**, 043528 (2013).
- [16] Rodrigo Maier, Francesco Pace and Ivano Damião Soares, Phys. Rev. D **88**, 106003 (2013).
- [17] P. Hořava, Phys. Rev. D **79**, 084008 (2009).
- [18] G. Calcagni, JHEP **0909**, 112 (2009).
- [19] R. Brandenberger, Phys. Rev. D **80**, 043516 (2009).
- [20] C. Charmousis, G. Niz, A. Padilla and P.M. Saffin, JHEP **0908** 070 (2009).
- [21] Thomas P. Sotiriou, J. Phys. Conf. Ser. **283** 012034 (2011).
- [22] Y. Misonoh, K. Maeda and T. Kobayashi, Phys. Rev. D **84**, 064030 (2011).
- [23] D. Blas, O. Pujolas and S. Sibiryakov JHEP **0910**:029 (2009).
- [24] C. Bogdanos, Emmanuel N. Saridakis, Class. Quant. Grav. **27** 075005 (2010).
- [25] K. Koyama and F. Arroja, JHEP **1003** 061 (2010).
- [26] T. P. Sotiriou, M. Visser and S. Weinfurtner, JHEP **0910** 033 (2009).
- [27] Jorge Bellorín, Alvaro Restuccia and Adrán Sotomayor, Phys. Rev. D **87**, 084020 (2013).
- [28] Antonios Papazoglou and Thomas P. Sotiriou, Phys. Lett. B **685** 197-200 (2010).
- [29] Yi-Fu Cai and Emmanuel N. Saridakis, JCAP **0910** 020 (2009).
- [30] V. I. Arnold, *Mathematical Methods of Classical Mechanics* (Springer, 1989).
- [31] M. Berry, AIP Conf. Proc. **46**, 16-120 (1978).
- [32] M. Abramowitz and I. Stegun, *Handbook of Mathematical Functions*, NBS Applied Math. Series 55 (National Bureau of Standards, Washington, DC, 1964).
- [33] A. N. Kolmogorov, in *Stochastic Behaviour in Classical and in Quantum Hamiltonian Systems*, eds. G. Casati e J. Ford, Lecture Notes in Physics Vol. 93 (Springer-Verlag, Berlin, 1979); V. I. Arnold, Russ. Math. Surv. **18**, 9 (1963); J. Moser, Nachr. Akad. Wiss. Goett., Math.-Phys. Kl. IIa, **1** (1962).
- [34] G. M. Zaslavsky, R. Z. Sagdeev, D. A. Usikov and A. A. Chernikov, *Weak Chaos and Quasi-Regular Patterns* (Cambridge University Press, 1991).
- [35] R. Maier, I. Damião Soares and E. V. Tonini, Phys. Rev. D **79**, 023522 (2009).
- [36] H. P. Oliveira, A. M. Ozorio de Almeida, I. Damião Soares and E. V. Tonini, Phys. Rev. D **65**, 083511 (2002).
- [37] R. Maier, I. Damião Soares and E. V. Tonini, Class. Q. Gravity, **32**, 235001 (2015).
- [38] D. M. Y. Sommerville, *The Elements of Non-Euclidean Geometry* (Dover, New York, 1958).
- [39] H. Waalkens, A. Burbanks and S. Wiggins, J. Phys. A: Math. Gen. **37**, 257 (2004).
- [40] J. Guckenheimer and P. Holmes, *Dynamical Systems and Bifurcations of Vector Fields* (Springer, New York, 1983).
- [41] S. Wiggins, *Global Bifurcations and Chaos* (Springer, Berlin, 1988).
- [42] A. J. Lichtenberg and M. A. Leiberman, *Regular and Chaotic Dynamics* (New York, Springer, 1992).
- [43] Juan M. Aguirregabiria, Dynamics Solver, <http://tp.lc.ehu.es/jma.html>.